A Physical Index Towards Real Time Monitoring of Potential Whale Habitats from Space

Will Perrie, Hui Shen, Jing Tao and Rick Danielson

Fisheries and Oceans Canada
Bedford Institute of Oceanography
Dartmouth, Nova Scotia, Canada
B2Y 4A2

2023

Canadian Technical Report of
Fisheries and Aquatic Sciences 3533

Fisheries and Oceans Canada | Pêches et Océans Canada

Canada

Canadian Technical Report of Fisheries and Aquatic Sciences

Technical reports contain scientific and technical information that contributes to existing knowledge but which is not normally appropriate for primary literature. Technical reports are directed primarily toward a worldwide audience and have an international distribution. No restriction is placed on subject matter and the series reflects the broad interests and policies of Fisheries and Oceans Canada, namely, fisheries and aquatic sciences.

Technical reports may be cited as full publications. The correct citation appears above the abstract of each report. Each report is abstracted in the data base *Aquatic Sciences and Fisheries Abstracts*.

Technical reports are produced regionally but are numbered nationally. Requests for individual reports will be filled by the issuing establishment listed on the front cover and title page.

Numbers 1-456 in this series were issued as Technical Reports of the Fisheries Research Board of Canada. Numbers 457-714 were issued as Department of the Environment, Fisheries and Marine Service, Research and Development Directorate Technical Reports. Numbers 715-924 were issued as Department of Fisheries and Environment, Fisheries and Marine Service Technical Reports. The current series name was changed with report number 925.

Rapport technique canadien des sciences halieutiques et aquatiques

Les rapports techniques contiennent des renseignements scientifiques et techniques qui constituent une contribution aux connaissances actuelles, mais qui ne sont pas normalement appropriés pour la publication dans un journal scientifique. Les rapports techniques sont destinés essentiellement à un public international et ils sont distribués à cet échelon. II n'y a aucune restriction quant au sujet; de fait, la série reflète la vaste gamme des intérêts et des politiques de Pêches et Océans Canada, c'est-à-dire les sciences halieutiques et aquatiques.

Les rapports techniques peuvent être cités comme des publications à part entière. Le titre exact figure au-dessus du résumé de chaque rapport. Les rapports techniques sont résumés dans la base de données *Résumés des sciences aquatiques et halieutiques.*

Les rapports techniques sont produits à l'échelon régional, mais numérotés à l'échelon national. Les demandes de rapports seront satisfaites par l'établissement auteur dont le nom figure sur la couverture et la page du titre.

Les numéros 1 à 456 de cette série ont été publiés à titre de Rapports techniques de l'Office des recherches sur les pêcheries du Canada. Les numéros 457 à 714 sont parus à titre de Rapports techniques de la Direction générale de la recherche et du développement, Service des pêches et de la mer, ministère de l'Environnement. Les numéros 715 à 924 ont été publiés à titre de Rapports techniques du Service des pêches et de la mer, ministère des Pêches et de l'Environnement. Le nom actuel de la série a été établi lors de la parution du numéro 925.

Canadian Technical Report of
Fisheries and Aquatic Sciences 3533

2023

A Physical Index Towards Real Time Monitoring of Potential Whale Habitats from Space

by

Will Perrie, Hui Shen, Jing Tao and Rick Danielson

Science Branch
Maritimes Region
Ocean Ecosystem Science Division
Fisheries and Oceans Canada
Bedford Institute of Oceanography
PO Box 1006
Dartmouth, Nova Scotia,
B2Y 4A2

Cat. No. Fs97-6/3533E-PDF ISBN 978-0-660-43487-2 ISSN 1488-5379

Correct citation for this publication:

Perrie, W., Shen, H., Tao J., and Danielson, R. E. 2023. A Physical Index Towards Real Time Monitoring of Potential Whale Habitats from Space. Can. Tech. Rep. Fish. Aquat. Sci. 3533: v + 35 p.

Contents

Abstract

Perrie, W., Shen, H., Tao J., and Danielson, R. E. 2023. A Physical Index Towards Real Time Monitoring of Potential Whale Habitats from Space. Can. Tech. Rep. Fish. Aquatic Sci. 3533: v + 35 p.

The marine physical environment is a fundamental driving force for the marine ecosystem, which largely defines the living conditions of marine mammals. Persistent physical processes contribute to maintaining a healthy functioning ecosystem, including the habitats of numerous whale species. In recent years, North Atlantic Right Whales (NARWs) have been using the Gulf of St. Lawrence (GSL), a highly productive marine area, as a feeding ground in summer. To protect these endangered NARWs from potential risk posed by intensive fishing and shipping activities in this area, continuous monitoring of the whale habitat is needed. In this report, high resolution remote sensing data is adapted to monitor physical processes in the GSL whale habitat. Indexes are developed from data to provide a consensus evaluation of the physical conditions and their variations. These indexes are useful to understand historical variations in the physical conditions of the current whale habitat, and also useful to predict whale gathering patterns in the near future, providing a new tool for the management of the GSL whale habitat.

Key words: Gulf of St. Lawrence, North Atlantic Right Whales, Whale Habitat, Gaspé Current, Remote sensing, Altimeter, Synthetic Aperture Radar

Résumé

Perrie, W., Shen, H., Tao J., and Danielson, R. E. 2023. A Physical Index Towards Real Time Monitoring of Potential Whale Habitats from Space. Can. Tech. Rep. Fish. Aquat. Sci. 3533: v + 35 p.

Le milieu physique marin est une force motrice fondamentale de l'écosystème marin, qui définit en grande partie les conditions de vie des mammifères marins. Les processus physiques persistants contribuent au maintien d'un écosystème sain et fonctionnel, y compris les habitats de nombreuses espèces de baleines. Depuis quelques années, les baleines noires de l'Atlantique Nord (BNAN) utilisent le golfe du Saint-Laurent (GSL), une zone marine très productive, comme aire d'alimentation en été. Pour protéger ces baleines en voie de disparition des risques liés aux activités intensives de pêche et de navigation dans cette zone, une surveillance continue de l'habitat des baleines est nécessaire. Dans ce rapport, on a adapté les données de télédétection à haute résolution pour surveiller les processus physiques dans l'habitat des baleines dans le GSL. On a élaboré des indices en fonction des données pour fournir une évaluation consensuelle des conditions physiques et de leurs variations. Ces indices sont utiles pour comprendre les variations historiques des conditions physiques de l'habitat actuel des baleines ainsi que pour prédire les schémas de rassemblement des baleines dans un avenir rapproché, fournissant ainsi un nouvel outil pour la gestion de l'habitat des baleines du golfe du Saint-Laurent.

Mots-clés : golfe du Saint-Laurent, baleines noires de l'Atlantique Nord, habitat de la baleine, courant de Gaspé, télédétection, altimètre, radar à synthèse d'ouverture

1. Introduction

1.1 Executive Summary

Physical indexes are developed from remote sensing data to monitor variations of the Gaspé Current, a dominant feature of the western Gulf of St. Lawrence (GSL) circulation. The variations of these physical indexes are found to correlate well with the distribution patterns of zooplankton and North Atlantic Right Whales in the GSL. These indexes are based on sea surface heights measured from satellite altimeter and sea surface roughness from satellite synthetic aperture radar (SAR). Various indexes are proposed to characterize the variations of the extension and intensity of the Gaspé Current. The indexes are applied to the Gaspé Current northern branch, located in lower estuary areas close to Anticosti island, and also the southern branch, located in the southern GSL. The physical indexes derived from satellite altimeter data perform better in the northern GSL, whereas SAR is found to be especially useful in the southern branch, thereby providing a full picture of the Gaspé Current front, including precise outlines of the boundary of the Gaspé Current plume in the southern GSL.

Satellite remote sensing provides a unique tool to monitor the oceanic circulation in whale habitat areas of the GSL. It is found that during the 2015-2019 period, scattered zooplankton and whale aggregation patterns in the southern branch correspond to years of an intensified Gaspé Current, whereas a more confined distribution pattern corresponds to a more normal, weak Gaspé Current strength. Our analysis confirms that the river discharge has an important role in the intensity of the Gaspé Current and associated ecosystem responses. In future, these indexes can be extended in time, based on available satellite observations, to provide a better view of inter-annual variations in the dynamical environment of the whale habitat areas, and to predict future changes in whale habitat.

1.2 Technical Summary

Two methods are developed to define indexes to quantify variations in the key physical processes of the Gulf of St. Lawrence, based on satellite altimeter and satellite synthetic aperture radar measurements.

The *first* method is based on sea surface level measurements from altimetry, with a focus on the dominant ocean circulation system – the Gaspé Current system. To characterize Gaspé Current variation, two indexes are developed. One index, denoted $\text{index}_{\text{volume}}$ (defined as $\sum_{i=1}^{n} \frac{SLA_i+SLA_{i+1}}{2} \times Distance_{i,i+1}$), is calculated from the SLA (sea level anomaly) along the entire extent of the northern track (about N49° ~ N50.5°), which links the amount of water flowing *through* that track. Eleven years of altimetry measurements (2010-2020) are analyzed. In general, the variation in $\text{index}_{\text{volume}}$ is positively correlated with river discharge (R = 0.54), the main driver of the Gaspé Current in the spring and summer. Another index, denoted $\text{index}_{\text{slope}}$ ($\sum_{i=1}^{n} \frac{SLA_i-SLA_{i+1}}{Distance_{i,i+1}}$), is linked to the intensity of the Gaspé Current. The variation of $\text{index}_{\text{slope}}$ is correlated with river discharge during the spring season (May and June). Overall, our results demonstrate that for the northern branch of the GSL, satellite altimetry data are capable of

monitoring the intensity and extension of the Gaspé Current. However, for the southern branch, altimetric indexes exhibit broader variations that cannot be directly linked to Gaspé Current variations. These results highlight that river discharge plays an important role in ocean dynamics of the Northwest Gulf.

The *second* method is based on the sea surface roughness measurements from SAR. Ocean circulation features, and in particular convergence and divergence patterns, can be obtained, benefiting from SAR's high-resolution two-dimensional sea surface roughness data. Feature identification is successfully adapted to provide knowledge of the ocean current systems, eddies, fronts, and other dynamical processes. An index based on the spatial anomalies and gradients of sea surface roughness is developed to retrieve frontal positions associated with the edges of current systems and boundaries of different water masses. This index is used to obtain the spatial extent of the Gaspé Current in the southern GSL, usually in the form of the Gaspé plume. Thus, spatial processing of SAR data is particularly useful for monitoring the development of ocean circulation systems in the Southern GSL.
Both altimeter and SAR are capable of providing data measurements in all-day and all-weather conditions. The combination of indexes from both platforms offers satellite remote sensing solutions for monitoring the physical dynamics across the entire GSL whale habitat region.

1.3 Preamble

Physical oceanographic conditions have profound impacts on ecosystems, and define the suitability of whale habitats. Knowledge of whale habitats is crucial for implementation of effective measures to monitor, protect and support the recovery of endangered NARWs and NABWs (North Atlantic Blue Whales). Traditional methods have relied on opportunistic observations and whale sightings from ships and aerial surveys.

Oceanographic conditions largely determine the prey availability (Cox et al., 2018), food sources, and thus, the suitability for whale habitat. Relevant conditions include mesoscale physical processes, such as ocean fronts, internal waves and eddies, which are important in zooplankton aggregation (Davies et al., 2014), food web modulations (Cullen et al., 2002), and nutrient supplies (Prairie et al., 2012). Previous work has highlighted the importance of ocean dynamics in modulating krill distributions (prey for NABWs) in the Northwest Atlantic (Plourde et al., 2016) and Calanus (prey for NARWs) in the southern GSL (sGSL) (Brennan et al., 2019). In recent years, the sGSL has become a NARW feeding ground (summer and fall), which puts significant pressure on shipping and fisheries, etc. due to ship-whale collisions, shipping noise, entanglements with fishing gear etc. For NABWs, a feeding ground is the Lower St. Lawrence estuary. Better knowledge of whale habitats is critical; substantial variations occur in prey biomass locations, on yearly and decadal timescales (Lehoux et al., 2020; Gavrilchuk et al., 2020), which determine whale habitat suitability and occurrence patterns.

Historical acoustic zooplankton surveys find that the Lower Estuary/Gaspé Current system acts as an important pathway and Calanus pump (Plourde and Runge, 1993) for zooplankton transportation and aggregation in the western GSL, defining whale distribution patterns (Zooplankton Database, 2020; Maps et al., 2014). Mesoscale oceanic dynamics are able to

aggregate whale prey into '*patches'*, which are attractive to the whales; This may explain why NARWs are mostly seen in the sGSL, although suitable foraging Calanus concentrations are also distributed elsewhere (WhaleMap, 2020; Plourde et al., 2019). Therefore, predictions of foraging habitats can be enhanced by remote sensing observations of mesoscale features. Our recent study funded by DFO SARMD mapped mesoscale phenomena in the Gulf of Maine (Shen et al., 2020).

During early stages of its life cycle, in springtime, Calanus mostly float in upper layers of the water column, with aggregation patterns that tend to be closely related to *upper ocean dynamics*. After June, the mature stage Calanus enters diapause in deeper waters. However, in sGSL, a large portion of Calanus continue their young active growing stage, floating in the upper layers (Plourde et al., 2001; Johnson et al., 2007). In this period, high-resolution remote sensing observations can infer Calanus abundancy and aggregation patterns.

SAR observations are available from the RADARSAT-2 satellite, and RADARSAT Constellation Mission (three new Canadian satellites), featuring 24-hour, high-resolution, all-weather observations, with unprecedented high revisit frequencies. Multiple satellite *altimeters* can provide complementary along-track high-resolution sea surface height measurements, with high revisit frequency, to monitor ocean fronts. Combined applications of SAR and *altimeter* satellites can provide novel tools to monitor and predict whale habitats.

High-resolution satellite observations also open the door for direct whale detection from space. This technology was validated by counting Southern Right Whales in a coastal bay of Argentina, and by gray whale detection using airborne radar off Santa Cruz, USA (Radford et al., 1994). Recently, we participated in the sGSL Dalhousie University SONOBUOY whale experiment (Dal-SONOBUOY), where we made preliminary progress for SAR detection of NARW.

This report aims to identify and monitor habitat suitability for NARWs and NABWs in GSL. Satellite remote sensing is unique in observing mesoscale processes, thereby providing a potential linkage between ocean dynamics, zooplankton and whale gathering patterns. *Our focus* is to develop indexes to predict whale habitat suitability, based on real-time, high-resolution, remotely sensed observations. Using these indexes, the spatial extents of potential whale habitats are *estimated* for the following weeks/months, providing guidance to management decision-makers.

1.4 General Ocean Dynamics in West GSL

The Gulf of St. Lawrence (GSL) is a semi-enclosed sea, which communicates with the Atlantic Ocean through Cabot Strait and the Strait of Belle Isle (Koutitonsky and Budgen, 1991). The Gulf is a combination of numerous deep troughs and shallow areas. The Laurentian Channel is a long, continuous trough, over 300 metres deep, that runs 1100 km from the edge of the continental shelf to the St. Lawrence Estuary. The Magdalen Shallows cover the southern part of the Gulf, occupying a rather wide and shallow plateau with depths that rarely exceed 80 m (Koutitonsky and Budgen, 1991; Han et al., 2004). The GSL is a special marine environment, which receives large amounts of freshwater drainage from Great Lakes and the St. Lawrence

Basin. Therefore, the main forcing for the circulation in the GSL is buoyancy forcing induced from the freshwater input (St. Lawrence river) and heat flux (Koutitonsky and Budgen, 1991). St. Lawrence River flow and surface heat fluxes exhibit strong seasonal variability (Benoit et al., 1985; Koutitonsky and Budgen, 1991). The runoff starts to rise in March, reaching a maximum in May at about 20 000 m^3/s, and decreasing from June to September, to a value of about 13 000 m^3/s. Maximum heat flux values are reached in June. In winter, the GSL is mostly ice – covered. Furthermore, other factors are also known to affect the GSL system, such as tidal forcing, and both local and large-scale meteorological forcing over the Gulf and additional oceanic forcing from the Atlantic (Koutitonsky and Budgen, 1991).

A significant feature of near surface circulation in the GSL is the Gaspé Current (also denoted, GC). The GC is a strong coastal current, which develops in the St. Lawrence Estuary, reinforced by a southward coastal current at the mouth of the Estuary, and intensifying as it moves around the Gaspé Peninsula (El-Sabh 1976; Koutitonsky and Budgen, 1991; Sheng, 2001). A cyclonic gyre is formed in the northwest GSL during the summer. A portion of the GC recirculates cyclonically within the northwest GSL and then combines with a barotropic westward jet (Labrador Shelf Current) along the Quebec North Shore (Koutitonsky and Budgen, 1991; Sheng, 2001). The main GC branch continues eastward along the Gaspé Peninsula, carrying buoyant estuarine waters onto the Magdalen Shallows (Benoit et al., 1985; Sheng, 2001). The GC reflects the river flow, being strong and warm in the summer and cold and weak in the winter (Benoit et al., 1985). An overview of relevant processes and factors is given in Figure 1.

1.5 The Zooplankton Pump – Gaspé Current

Historical acoustic zooplankton surveys in 2018 and 2019 found that the Gaspé Current can be an important pathway for zooplankton transportation and aggregation characteristics in the eastern GSL, defining whale distribution and behavior patterns (Cox et al., 2018; Zooplankton Database, 2020). At the same time, mesoscale oceanic dynamics are able to aggregate whale prey into patch – like formations, which are attractive to the whales. This may help to explain why NARWs have been seen mostly (and by far) in the sGSL, despite the fact that suitable foraging concentrations of Calanus are likely present in other areas where DFO has surveyed (a finding from the annual field surveys since 2017). Therefore, information on mesoscale oceanographic features can enhance our ability to predict suitable foraging habitats. Satellite remote sensing data are capable of observing these small-scale mesoscale dynamics. A recent study funded by DFO SARMD mapped these mesoscale phenomena, particularly internal wave distributions in the Gulf of Maine (Maps et al., 2014).

During early stages of its life cycle, from April to June, Calanus mostly float in the upper layers of the water column; thus, its aggregation patterns are closely related to upper layer ocean dynamics. After June, the mature stage Calanus enters diapause in deeper water column layers. However, in sGSL, a big portion of Calanus continues to float in the upper layers, in their young actively growing stage. High-resolution remote sensing is particularly useful during this period, to infer Calanus abundancy and aggregation patterns.

1.6 Scientific Questions and the Hypothesis

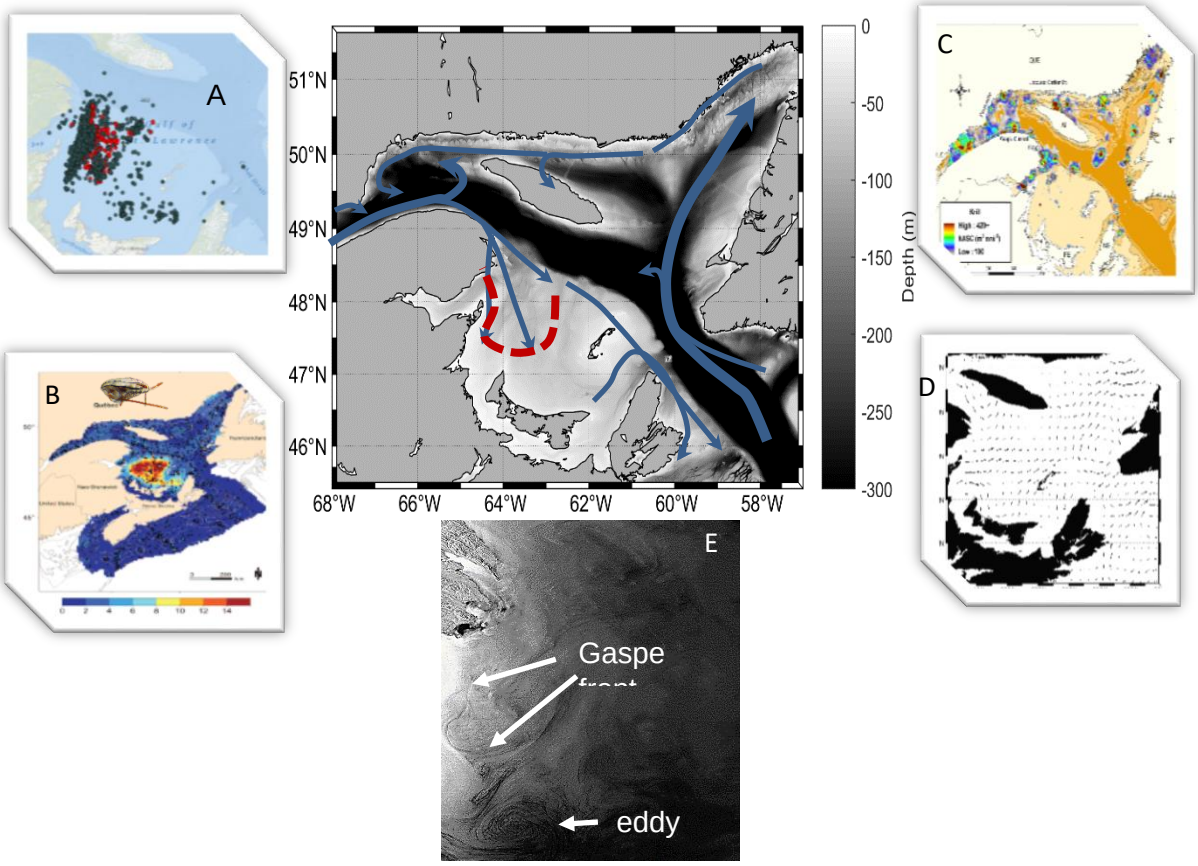

Figure 1. Map of project area (center panel). Shading represents ocean bathymetry; blue arrows represent ocean circulation; red dashed curve shows the Gaspé Current front. Four sub-images are: (A) whale sightings during 2016-2019 (WhaleMap, 2020), (B) maximum Calanus spp. - NARW prey energy density from DFO zooplankton surveys (Plourde et al. 2019), (C) composite krill distribution - NABW prey aggregation from acoustic surveys (McQuinn et al., 2015), (D) ocean circulation including Gaspé Current extension from satellite altimetry, (E) SAR snapshot of a Gaspé front and eddy.

The GSL is a habitat area for endangered NARWs and NABWs. Traditionally, the Lower St. Lawrence estuary has been used by NABWs as a feeding ground. In recent years, the sGSL has been frequently visited by NARWs. Local oceanographic conditions define the habitat. The Gaspé Current is a main fresh water pathway to sGSL, acting as a “pump”, providing Calanus from deep water; high density, large-scale krill aggregations are observed in DFO’s acoustic surveys off the Gaspé Peninsula. The applicability of the Gaspé Current front as an index for food availability may be investigated/implemented as a *predictor* of *whale* habitat and gathering patterns. Other mesoscale processes, including central GSL recirculation patterns, eddies and internal solitary waves, can also contribute to local convergence of zooplankton, promoting the formation of high concentration zooplankton patches, which are of particular interest to the whales. The high concentration patches are formed through small-scale biological-physical

interactions in which zooplankton movements interact with small-scale ocean convergence/divergence features. These ocean mesoscale features include ocean fronts, internal waves, eddies etc. (Prairie et al., 2012), thereby acting as potential indicators of high concentration patches of surface-dwelling zooplankton aggregations (Davies et al., 2014) and food web modulations (Cullen et al., 2002). It is difficult to monitor the Gaspé Current pathway and mesoscale features using traditional ship and aircraft surveys. Satellite SAR and altimeters can give high-resolution, all-weather and high-revisit-frequency observations, providing novel tools to help detect potential whale habitats.

Satellite detection of the Gaspé Current and *other mesoscale processes* fills a gap in observations of small-scale physical features, which can be important for identifying Calanus transport to key locations (e.g. the Gaspé Current pathway into the sGSL or along the Laurentian Channel) and for zooplankton aggregation. *Remote sensing data* can provide important '*ground-truth*' data to the operational ocean model; as well as an alternative, independent way to develop a Gaspé Current index, directly from satellite observations.

1.7 Management needs

There is a strong need for management guidance in efforts to protect NARWs and NABWs, especially the more urgent need to protect the NARWs. For DFO, the overarching objective is to understand the processes that drive variability in NARW foraging habitats, in sGSL, and in other areas that have not yet been identified. Currently, the DFO *response* to risk for NARWs, is to close fisheries and set speed limits.

Information, such as derived from this report, can be used for decisions regarding ship traffic and fishery closures, as directly linked to the suitability of western GSL whale habitats. Physical oceanographic processes contribute to large scale aggregation and local scale convergence of whale pray – zooplankton; when prey patches have scattered distributions, whale distributions are wide and more unpredictable. *Additional products* are independent data for validation and interpretation of whale habitat changes, zooplankton survey data and DFO numerical forecasting model results. This research supports SARA recovery strategies for NARWs "1,2 Reduce mortality/ injury from ship strikes and fishing gear", high priority recovery measures of "12c,d Identify the presence of additional high-use habitat" and supports NABWs for urgent priority of recovery strategy "3. Implement a research/ monitoring program to fill knowledge gaps about zooplankton distribution/ concentration/ variability and other prey of the blue whale" (SARA, 2020).

On 'longer' timescales, remotely sensed products are beneficial to support better understanding of climatology, including past changes and future projections of whale habitat suitability. On 'shorter' timescales, they reveal present oceanographic conditions necessary for immediate decision-making.

2. Data and Observations

This project employs in situ and polar orbiting satellite data, including swath coverage by the RADARSAT-2 synthetic aperture radar (SAR) and several altimeters, whose along-track sea level estimates have been calibrated across platforms. Coverage of the Gulf of St. Lawrence begins well prior to 2015. In situ observations include the whale sighting database of the North Atlantic Right Whale Consortium (NARWC), a component of which is held at the Bedford Institute of Oceanography, and zooplankton surveys conducted by the Bedford Institute of Oceanography and Maurice Lamontagne Institute.

2.1 SAR

Synthetic aperture radar (SAR) is an active imaging system which measures surface roughness of the target. Over the water surface, SAR is particularly sensitive to the capillary-wave scale roughness, depending on the frequency of the radar system. For example, C band (5.3GHz) SAR is sensitive to the capillary wavelength of 5.3 cm. Any processes and targets which can change the corresponding wave properties will show up in the image of SAR measurements, including ocean fronts. The unique advantage of SAR is its horizontal high spatial resolution in two dimensions. Benefiting from the special synthetic technology of its antenna, modern SAR's pixel resolution is generally less than 50m. The high spatial resolution makes SAR particularly useful to monitor mesoscale and submesoscale dynamical ocean features.

Over the years, many SAR systems have been developed. In particular, Canada is a recognized leader in this technology, for three generations of satellites: RADARSAT-1 (R1), RADARSAT-2 (R2) and RADARSAT Constellation Mission (RCM). The RADARSAT SAR series all operate at C-band frequency (5.3GHz). Together, these satellites have accumulated continuous data time series, beginning in 1996 to the present (R1 1996-2013, R2 2007-, and RCM 2019-). In year-1 study of this project, RADARSAT-2 SAR is used to develop a suitable method to identify ocean fronts. The method is expanded to R1 and RCM data in ongoing years of the project.

Unlike continuously scanning instruments, SAR images are acquired by request. Figure 1 shows a subset of the footprints of all R2 SAR data requests from 2015-2019. Altogether, there are about 1000 images in the areas of interest for the current project – western Gulf of St. Lawrence (the red polygon shown in the figure). Including orders generated by this project, SAR data coverage continues to increase over time.

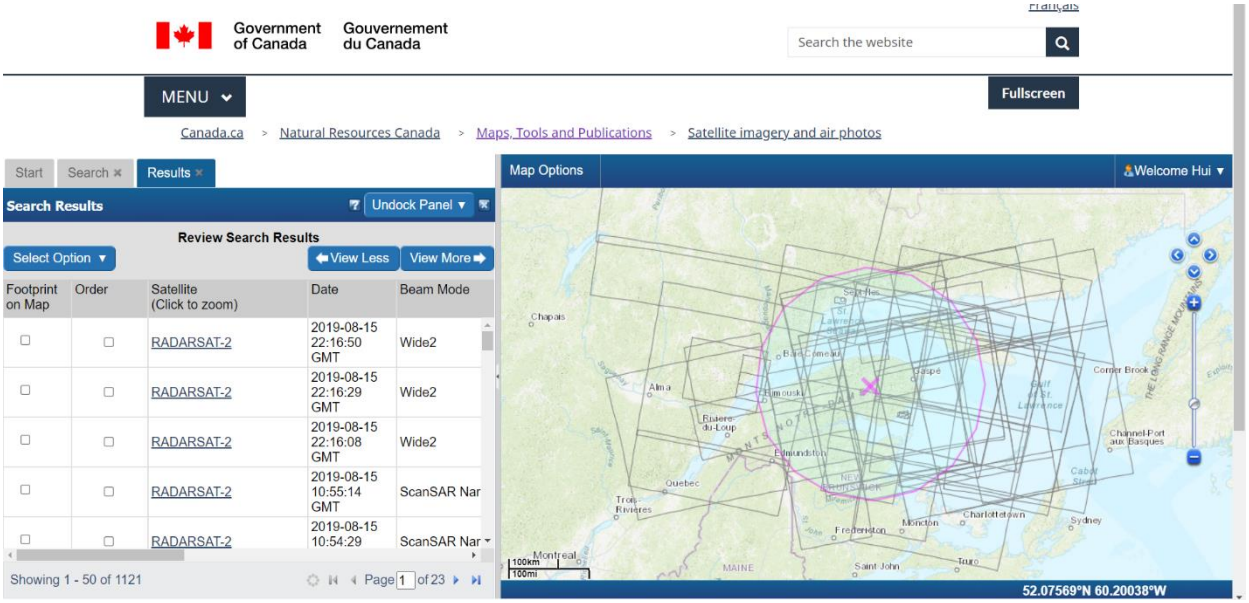

Figure 2. The NRCAN EODMS website (www.eodms-sgdot.nrcan-rncan.gc.ca) showing 50 of 1121 RADARSAT-2 SAR footprints during May to mid-August of 2015 to 2019 with coverage over a circular region covering the western Gulf of St. Lawrence (purple circle).

Characteristics of ocean surface roughness (cm-scale waves) are mapped at better than 100-m resolution. At this resolution, an assortment of larger coherent structures and processes are imaged at the ocean surface, as illustrated in the SAR Marine User's Manual (NOAA 2004). Note that this project targets mesoscale fronts and eddies that identify attractive feeding grounds; specifically, filamentary structures in SAR imagery are associated with coherent horizontal and vertical circulation along which whale prey can accumulate. Therefore, one challenge is that a range of different processes may be captured in each SAR scene. Gridded surface wind and rain estimates are first added to each scene to enhance our ability to focus on ocean processes. An analysis methodology is then applied to better resolve the eddy and filamentary structures of interest.

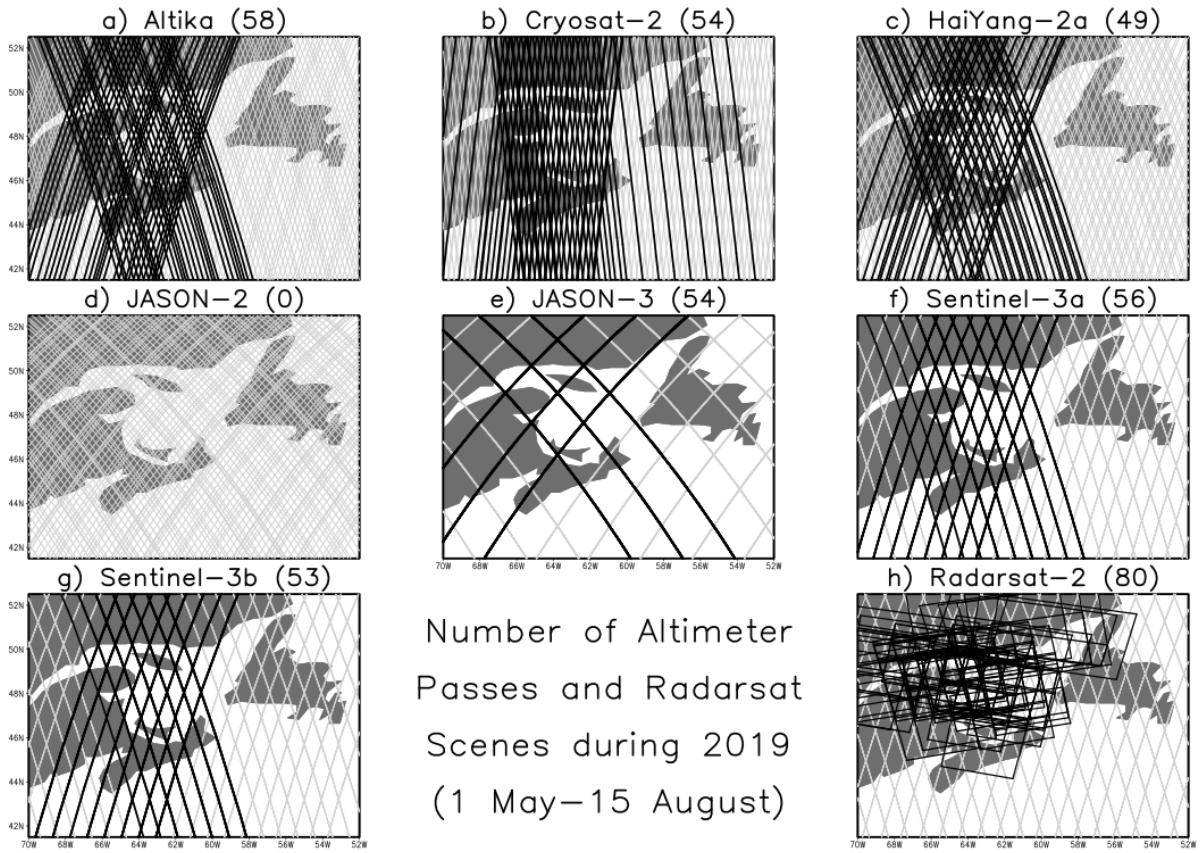

Figure 3. Multiple altimeter and RADARSAT-2 SAR overpasses that image the western Gulf of St. Lawrence between 1 May and 15 August, 2019. The number of overpasses with data is given in brackets for: a) Altika, b) Cryosat-2, c) HaiYang-2a, d) JASON-2, e) JASON-3, f) Sentinel-3a, g) Sentinel-3b, and h) RADARSAT-2 satellites. The RADARSAT-2 scenes are shown by black boxes and the altimeter ground tracks that contain data over the Gulf region are shown by black lines (i.e., complete morning or afternoon ground track segments, whereas grey lines are the segments without Gulf coverage).

Real-time SAR data access is provided by Natural Resources Canada (NRCAN), which has previously established an Earth Observation Data Management System (EODMS) whereby several methods have been automated, for a multi-step procedure to request SAR scenes to be placed on an NRCAN server, and after some delay, to inform users of where to download data. User delay is now reduced using a python script, to search, order, and download SAR data in a single step. Several types of SAR and optical satellite archives are available from the NRCAN archive; this project begins with RADARSAT-2 wide-swath acquisitions from May-August 2015-2020 that overlap the circular area shown in Figure 2.

Overall, the RADARSAT-2 SAR offers good warm season coverage of the western Gulf during 2015-2020, at intervals ranging from shorter than daily to longer than weekly. Wide swath coverage has become somewhat better in recent years, with 80 scenes available in 2019 (Figure 3) versus 48 scenes in 2015 (not shown).

2.2 Altimeter

The altimeter satellite data have been applied to study oceanic water-motion features in the ocean under all weather conditions (Joseph, 2013). In previous studies, sea level and surface current variability have been investigated primarily using altimeter data in different regions (Fu and Chelton, 2001; Bonjean and Lagerloef, 2002; Yu et al., 2014, Han, 2004). Satellite altimetry measurements provide the sea surface level relative to a reference ellipsoid, the marine geoid. Geostrophic surface currents therefore can be calculated from the slopes of the sea surface in the global ocean. Satellite altimeter data have been used to characterise sea level and surface current variability in the Gulf of St. Lawrence (Han et al., 2002; Han, 2004). The satellite altimeter data employed in this study are taken from the CMEMS website (Copernicus Marine Environment Monitoring Service, https://marine.copernicus.eu/).

By convention, a minimum of three or four altimeters is considered necessary to identify individual mesoscale eddies (CMEMS 2020). At least four altimeters have provided coverage of the Gulf of St. Lawrence during the summer months of 2015-2019. The best coverage was during 2019 (Figure 3), with JASON-3 and two Sentinel-3 satellites on repeating tracks, and three other platforms. The Copernicus Marine Environment Monitoring Service (CMEMS) makes available a reprocessing of altimeter missions that calibrates instruments to a TOPEX/JASON reference time series. Reprocessing (CMEMS_008_062) is not performed in real time (i.e., the March 2020 update contains data through mid-October 2019), although real-time products (CMEMS_008_044) are available. This reprocessing is instead intended for assimilation (e.g., in historical reanalyses) and includes selected variables, such as smoothed and unsmoothed along-track sea surface height (SSH) anomaly data. This project employs the smoothed product, with a shortwave cutoff of 65 km (Figure 7), so data are provided at 1-s (or 7-km) resolution; but altimetry is mainly expected to capture broader mesoscale height variations, within which filamentary structures exist. The SSH is defined following the geodesic convention (height above the WGS84 ellipsoid in a tide-free system) and SSH anomalies are given relative to a time-mean sea surface (Rio et al. 2014). Ocean tidal and atmospheric corrections are also applied to all SSH anomalies; but for any global correction, these may be slightly incomplete in the Gulf of St. Lawrence.

Five altimeter platforms are employed in Section 5 to obtain long timeseries altimetric indexes: Jason-2/3 (J2/3), Sentinel-3A/B (S3A/B), and ENVISAT (EN). These satellites repeat their ground track crossings of the Gaspé Current every 9.9156, 27 and 35 days, respectively. The CMEMS sea level height anomaly (SLA) product is the absolute dynamic topography minus the mean dynamic topography (MDT). The MDT is the mean of the surface height relative to a time-mean ellipsoid. It is computed on a regular grid and combines data from all available satellites. The J2 data were collected during a period from May 2009 to May 2016 and J3 data were collected from June 2016 to October 2019. The S3A/B data were collected during June 2016 to October 2018. The EN data were collected during 2002 to 2010. To monitor whale habitat, we focus on the 7-km along-track SLA data during six months per year (May to October). The J2/3 data were collected along an ascending track on the northern branch (Figure 4a; N49^{o} ~ 50.5^{o})

in the northwest GSL. The EN data were collected along two descending tracks on the northern branch (Figures 4b, 4c). The S3A/B and EN data were collected along a descending track on the southern branch (Figure 4d; N47° ~ 49°) in the northwest GSL.

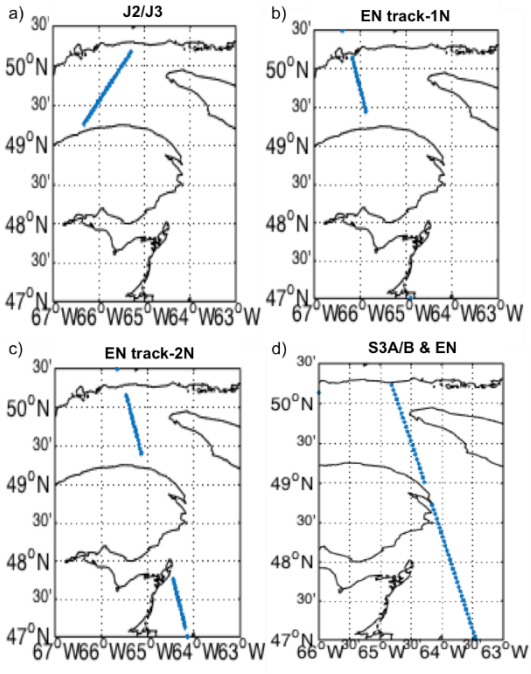

Figure 4. Gulf of St. Lawrence altimetric ground tracks of (a) Jason-2/3 (J2/3), ENVISAT (b) track-1 North (EN track-1N) and (c) track-2 North (EN track-2N), and (d) Sentinel-3A/B and ENVISAT southern coverage (S3A/B & EN).

2.3 River run-off data

The monthly mean runoff data of the St. Lawrence River were obtained from SLGO (St. Lawrence Global Observatory, https://ogsl.ca/en/freshwater-runoffs-quebec-city-application/). The runoff data are estimated using an empirical relationship between the St. Lawrence River discharge and the water level at Neuville, Quebec (Bourgault and Koutitonsky, 1999). The highest monthly mean runoff of the year is typically in May, and in the past two decades, peak runoff of over 22 000 m^3/s occurred during May in 2011, 2017 and 2019.

2.4 Ocean color and SST data

MODIS-Aqua satellite data are available from the NASA OceanColor Data website (https://oceandata.sci.gsfc.nasa.gov/). The spatial resolution of MODIS Level 3 sea surface temperature (SST) is 4 km and the daily SST product was downloaded and collocated with altimeter data. Because the MODIS infrared sensor is partially obscured by cloud cover, an integrated SST data product provided by the Group for High-Resolution Sea Surface Temperature (GHRSST) was also used in this study. GHRSST products combine infrared and

microwave SST data products from several sensors and resolve gaps in infrared SST products by blending and interpolation (GHRSST user manual). The daily GHRSST level 4 SST with the spatial resolution ~1 km were used in this study. A cursory examination of MODIS and GHRSST SST indicates that they are broadly consistent with each other, although GHRSST is notably warmer over the northwest GSL on July 7th, 2019, for example.

The GHRSST SST was interpolated to altimetric ground tracks in order to compare SST and SLA profiles. Also, in situ SST measurements were obtained from a buoy at Rimouski, QC (02985, https://ogsl.ca/conditions/) and compared to the nearest GHRSST pixel. Based on selected collocations in May 2015-2019, the two measurements agree to within about one degree (Figure 5).

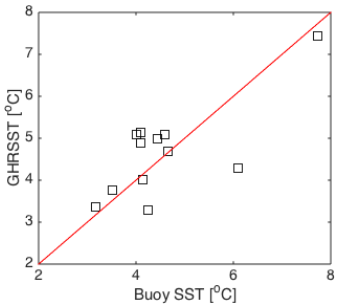

Figure 5. Scatter plot of GHRSST versus buoy SST data at the location of buoy 02985 (https://ogsl.ca/conditions/) near Rimouski, QC.

2.5 Whale sighting data

Occasional sightings of right whales in the Gulf of St. Lawrence increased in frequency after about 2013 (Kenney 2019). Among a total of over 50,000 right whale sightings from 1762 to 2018 in the North Atlantic Right Whale Consortium (NARWC) database (Kenney 2019), there are 3277 aerial survey and vessel-of-opportunity whale sightings (a combination of group and individual identifications), since 2015. A complementary DFO database contains 2660 sightings of right and blue whales in the Gulf of St. Lawrence (DFO 2020). Both the number of whales and number of whale groups are recorded in the North Atlantic Right Whale Consortium (NARWC) and DFO database, with a number of small groups of identical sightings separated by only a few minutes and less than a kilometer. Thus, possibly the same observer has reported the same whale more than once; and among multiple observers, some whales are counted more than once, either on the same day or on different days. However, neither whales nor observers are identified in the DFO database, which reports in local time, whereas duplicate sightings of the same whale may be possible to remove, for the 3277 NARWC sightings, which reports in UTC. Thus, 4 hr is added to the DFO data, when collocating with satellites. Reports for 2019 and 2020 continue to be assembled and quality controlled.

As there is partial overlap in the NARWC and DFO sightings, the NARWC are employed as a base and collocations in the DFO database are then omitted. Here, a collocation is taken to be a sighting of the same number of right or blue whales within 24h and 0.01° latitude and

longitude (this reduces the DFO data from 2660 to 1786). Some DFO sightings might have been of dead whales, but this is only recorded in the NARWC data (which reduces the NARWC data from 3277 to 3200). The total number of combined sightings is thus 1786 + 3200 = 4986. Below, we find an increase in the number of blue and right whale encounters before and after 2016/2017, and a varying dispersal of sightings in each summer month.

2.6 Zooplankton survey

DFO has operated the Atlantic Zone Monitoring Programme (AZMP) since 1998 with the aim of collecting and analysing the biological, chemical, and physical field data that are important for the understanding of the status and changes of the ocean. The key element of AZMP sampling strategy is that the oceanographic sampling should occur at fixed stations and along sections. The fixed stations are occupied about every two weeks, conditions permitting, and the sections are sampled in June and November. In the AZMP program, zooplankton are sampled from the bottom to the surface with a ringnet (0.75 m diameter, 200 µm mesh). An ecosystem status report on the state of phytoplankton and zooplankton is prepared every year. Data presented in this report are extracted from the latest report (Blais et al., 2021), which includes zooplankton analyses from 2000-2019.

The GSL is a coastal marine environment with a particularly high zooplankton biomass relative to other coastal areas, dominated by *Calanus* species (de Lafontaine *et al*., 1991). Historical data suggests that zooplankton abundance and biomass do not follow the same pattern as the concentration of Chlorophyll *a*. This absence of correlation between zooplankton and algal biomass has been observed in the GSL (de Lafontaine *et al*., 1991; Roy *et al*., 2000) and was attributed to the complex estuarine circulation pattern observed at the Gaspé Current (GC) and the Anticosti Gyre (AG). It is the objective of this report to try to fill this gap by monitoring the physical oceanographic conditions in the western Gulf of St. Lawrence from space, using satellites.

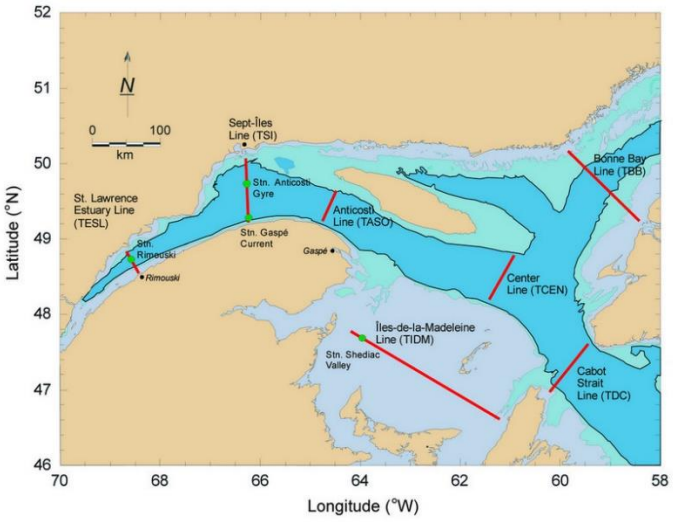

Figure 6. AZMP transects in the Gulf of St. Lawrence (dots: fixed stations, red lines: transects)

3. Methodology

3.1 SAR frontal feature detection

The use of SAR, both for visualizing and quantifying ocean surface processes, is relatively recent, but its potential has motivated the writing of the SAR Marine User's Manual (NOAA 2004). However, there is a longer history of exploring sun glint (Cox and Munk 1954), as well as more recent suggestions (Kudryavtsev et al. 2012) of a mechanistic relationship between the wave processes resolved by anomalies of sun glint and SAR normalized radar cross section σ_o. The SAR anomaly is thus defined as

$$(\sigma_o - <\sigma_o>)/<\sigma_o> \qquad (1)$$

where <> denotes a moving spatial average.

As an example of this calculation, scales of 400-1600 m are emphasized in Figure 7, where σ_o is at 400-m resolution, $<\sigma_o>$ is at 1600-m resolution, and successive half-size image reductions employ the digital filter of Koch (2004). Kudryavtsev et al. (2012) found a striking similarity between sun glitter and SAR anomaly patterns that were acquired a few hours apart. Just as an entire spectrum of wind waves may contribute to sun glitter (Cox and Munk 1954), Kudryavtsev et al. (2012) argue that breaking of larger waves contributes to the smaller waves detected by SAR. Moreover, they calculated convergence and divergence patterns that are also similar, in both the quasi-geostrophic and the wind-wave-current-imaging frameworks. Neither calculation is trivial, however, and in this project, it suffices to calculate equation (1) to highlight where there may be localized filaments of convergence, divergence, and vertical circulation.

3.2 Along track altimeter eddy detection

The reprocessing of altimetric data yields smooth along-track estimates of sea level, so broad mesoscale height variations are captured, but without any filamentary structure. Examples of cyclonic and anticyclonic eddies resolved by the Altika instrument are given in Figure 7. A broad anticyclonic center is observed at 49.5ºN, between the Gaspé Peninsula and Anticosti Island. The cyclonic center at 47.3ºN is associated with filaments of relatively stronger contrast. There is also the suggestion of a weak anticyclonic circulation at 48ºN; the area between these two eddies that may mark the boundary of the Gaspé Current. Thus, altimetry can be used to identify individual eddies, even when an eddy is not centered on the track.

Previous studies have indicated that satellite altimeter can be used for remotely sensed

measurements of ocean currents (Fu and Chelton, 2001; Bonjean and Lagerloef, 2002; Yu et al., 2014). Geostrophic surface currents are maintained by horizontal pressure gradients and are expressed as sea surface height slopes relative to the geoid. The u-component (u_s) and the v-component (v_s) of the geostrophic surface currents can be related to surface elevation ζ by the expressions (Yu et al., 2014):

$$u_s = -\frac{g}{f}\frac{\partial \zeta}{\partial y}; \quad (2)$$

$$v_s = -\frac{g}{f}\frac{\partial \zeta}{\partial x}, \quad (3)$$

in which, g is gravitational constant, and f is the Coriolis parameter. Therefore, the SLA slope can be used as a proxy for the intensity of the surface geostrophic current. In this study, different indexes have been proposed to examine the variation of the extension and intensity of the GC. As a proxy of the surface current intensity, $Index_1$ is proposed as the gradient between the maximum and minimum SLA along a satellite track. The basis for employing extreme SLA values is that the location of the Gaspé Current is known to periodically separate from its typical path around the Gaspé Peninsula (Koutitonsky and Bugden 1998). As a proxy of water discharge through the same profile, $Index_2$ is defined using the same values of extreme SLA.

The indexes are calculated as:

$$index_1 = \frac{SLA_{max} - SLA_{min}}{Distance_{\max\_min}} \quad (4)$$

$$index_2 = \frac{SLA_{max} + SLA_{min}}{2} \times Distance_{\max\_min} \quad (5)$$

where SLA_{max}, and SLA_{min} are the SLA maximum and minimum values along the track, respectively, and $Distance_{\max\_min}$ is the distance between the corresponding locations. In terms of units, $Index_1$ [cm/km] is linked to the GC velocity, whereas $Index_2$ [m×km] is linked to water discharge. In general, the correlation between $Index_1$ and $Index_2$ is weak. The indexes can be generalized in the following way:

$$index_{slope} = \sum_{i=1}^{n} \frac{SLA_i - SLA_{i+1}}{Distance_{i,i+1}} \quad (6)$$

$$index_{volume} = \sum_{i=1}^{n} \frac{SLA_i + SLA_{i+1}}{2} \times Distance_{i,i+1} \quad (7)$$

where n is the number of data along each track, SLA_i is a measured value. Therefore, $index_{slope}$ [m/km] is a cumulative value along the entire track, which can thereby be used to examine the GC intensity. By comparison, $index_{volume}$ [m km] is used to indicate the amount of water flowing through the track. It is noted that only the SLA profiles with over 70% available data were included in this study. We hypothesize that variations of the slope index will correlate well with variations in the river discharge index, to first order, if changes in the river discharge dominate the sea surface height changes.

4. Case study

It is possible to associate filamentary structures in SAR imagery with coherent horizontal and vertical circulation along which whale prey might accumulate. It is also valuable to confirm the associated type of eddies using altimetry, as ecosystem (zooplankton) communities have been known to vary with stratification (Waite et al. 2019). Thus, eddy and frontal structures may indicate a potentially attractive feeding ground for whales. For example, Figure 7 reveals a group of six right whales (purple box) that were sighted near a strong filament on the periphery of an anticyclone located to the northeast of this area.

There remains the challenge that a single SAR scene often captures numerous structures and processes (NOAA 2004). For instance, to the west of the northern anticyclone in Figure 7 is a region devoid of fine structure, possibly owing to upwelling and a more stable atmospheric boundary layer with little wind stress at the surface. Also, between this anticyclonic eddy and Anticosti Island is the signature of what might be an atmospheric internal wave-train. Nevertheless, by comparison to the backscatter, the SAR anomaly (Kudryavtsev et al. 2012) seems widely applicable as a case study for investigation, by “turning up the gain” for the ocean surface processes of interest.

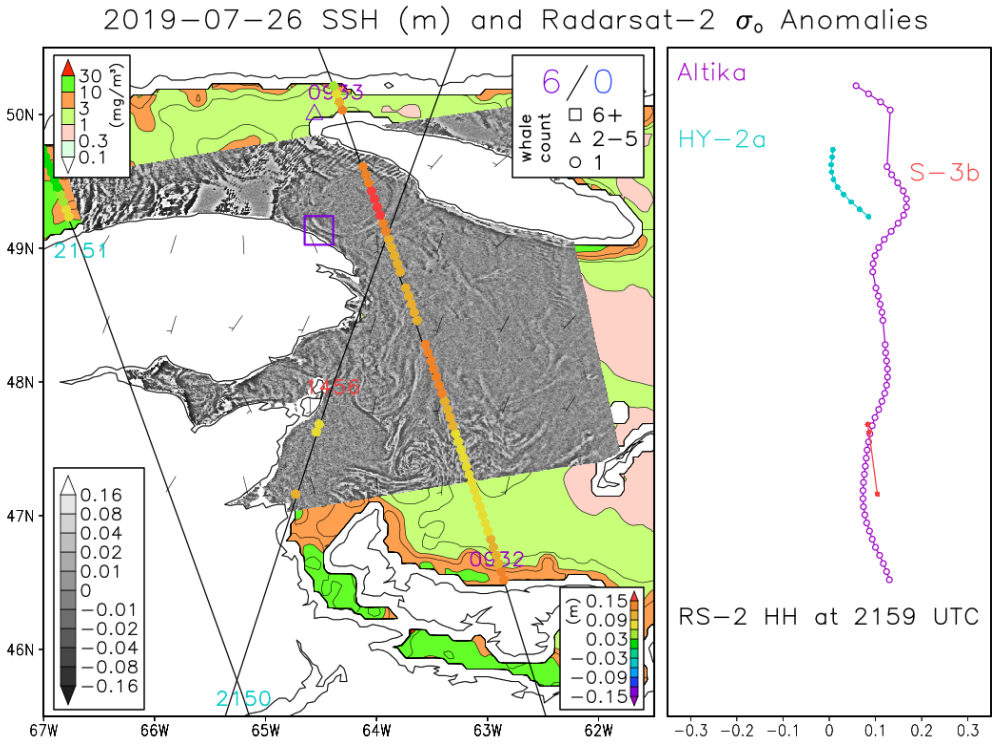

Figure 7. Example of filamentary structure captured by SAR, with SSH variations captured by collocated altimeters, on July 26, 2019. The left panel depicts the RADARSAT-2 backscatter anomaly (unitless, see lower-left legend grey scale) and time of overpass of the Altika (purple), HaiYang-2a (blue), and Sentinel-3b (red) altimeters (hour and minute bracket the ground tracks in black) with along-track SSH anomaly (m, lower-right legend showing the scale). Chlorophyll-a concentration (mg/m^3, upper-left legend colour scale) is based on

a merger of ocean colour satellite estimates (CMEMS_009_082). The location is shown for a group of six right whales that were sighted on this day (thick purple box, upper right legend scale). The right panel is a rotated view of the SSH anomaly tracks (i.e., as a function of latitude on the ordinate, and amplitude on the abscissa), with an identification of the SAR image (acquired at 21:59 UTC) as horizontally polarized (HH).

Altimetric processing within the Gulf of St. Lawrence involves a smoothed and tidally corrected anomaly, so both an overview and examples of these data are given for the ground tracks of Figure 4. Notations such as J2/3, EN track 1N, EN track-2N, S3A/B are defined in the Figure 4 caption. On the northern branch, a southward decreasing SLA feature is generally observed in J2/3 data (Figures 4a, and 8). Compared with the J2/3 northern track, the EN track-1N is located further upstream and the EN track-2N is located further downstream. Although S3A and EN ground tracks are more meridional, profiles of EN SLA along track-1N and track-2N are flatter than along J2/3 (Figures 4b, 4c, and 9). Some southward increasing SLA profiles are observed along the EN track-2N. On the southern branch, the SLA profiles display a strong spatial variation based on S3A and EN data (Figures 4d and 10). For J2/3 profiles, the histogram of the distance from the coastline to the southern ends of the tracks is shown in Figure 11. The mean of the distance is 12.9 km and the standard deviation is ±4.1 km. The southern end of the EN track is far from the coastline in the example in Figures 4b and 4c.

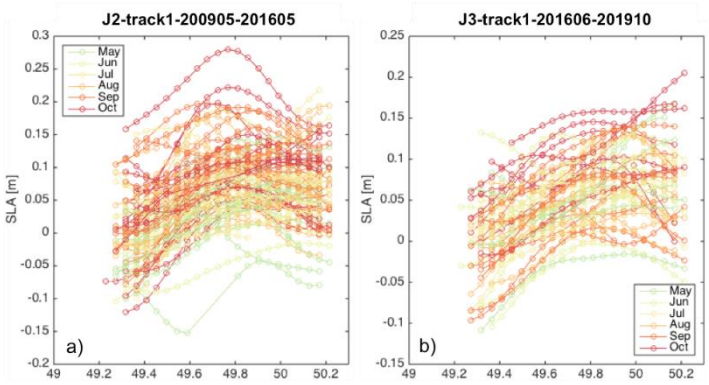

Figure 8. Distribution of SLA along the track derived from (a) Jason-2 and (b) Jason-3 between 2009 and 2019. Profiles are colored by month from May to October.

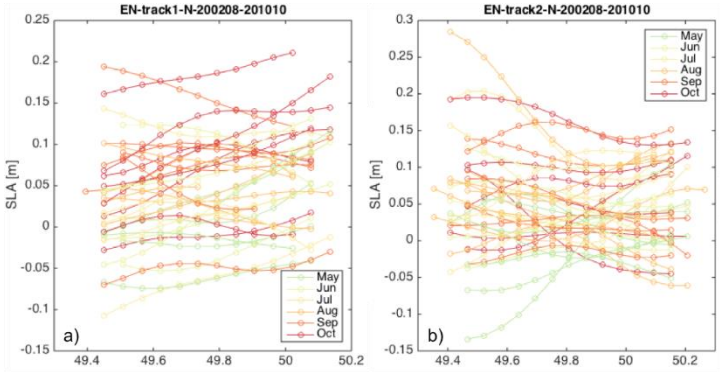

Figure 9. Latitudinal distribution of SLA along the (a) EN track-1N and (b) EN track-2N between 2002 and 2010. The profiles are colored by month from May to October.

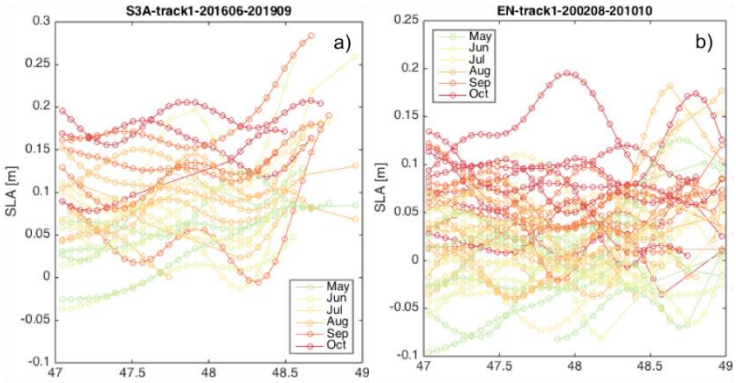

Figure 10. Latitudinal distribution of SLA along the (a) S3A and (b) EN tracks. The profiles are colored by month from May to October.

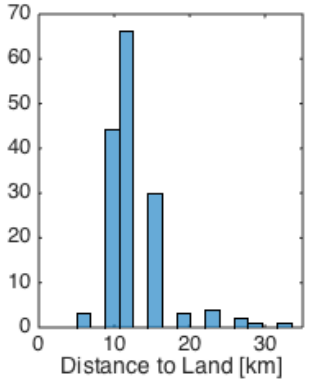

Figure 11. The histogram of the distance from the coastline to south end of profile derived from J2/3.

The GHRSST SST profiles along the two tracks were extracted. The SST profiles and SLA profiles were compared along tracks from 2016 to 2019. To investigate the usefulness of altimeter variations for density front detection, the SLA gradients were compared with the SST gradients. In general, the peaks of the SLA gradients are consistent with those of the SST gradients (Figures 12c, 12f, 13c, 13f). A clear density front was detected by the GHRSST SST pattern on August 30th, 2019. The altimeter S3A track also crosses this density front (Figure 13d). The steepest slopes of the SST and SLA profiles occur at the same locations (Figure 13f). This result supports our hypothesis that the SLA changes can be linked to GSL density fronts. Due to the complex GSL oceanic circulation, disagreements between the SLA and SST gradients are also observed for both northern and southern branches (such as Figure 13l).

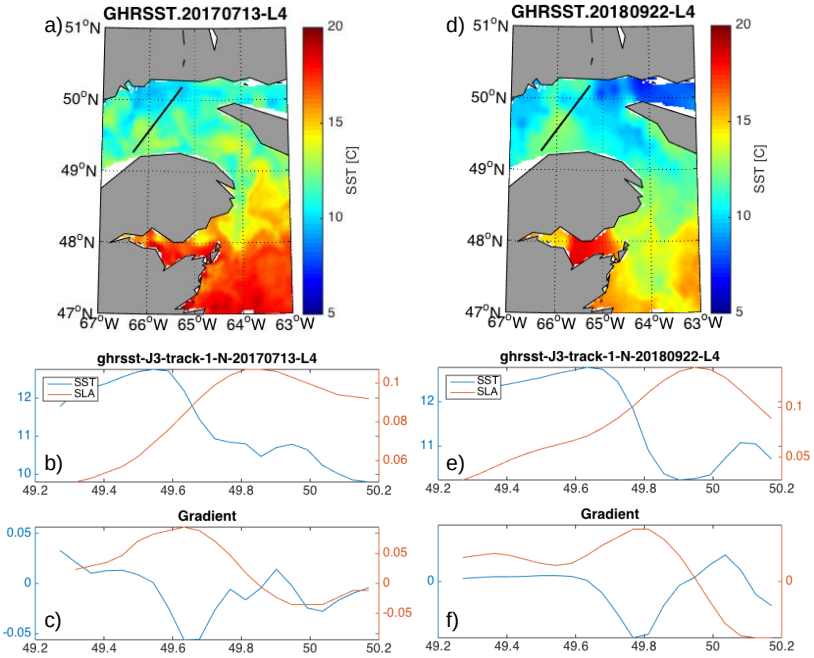

Figure 12. The GHRSST SST distribution on (a) July 13th, 2017 and (d) September 22nd, 2018. (b) and (e) latitudinal J2/3 SLA profile vs. corresponding GHRSST SST along the track (black line in map). (c) and (f) latitudinal SLA gradient vs. SST gradient along the track.

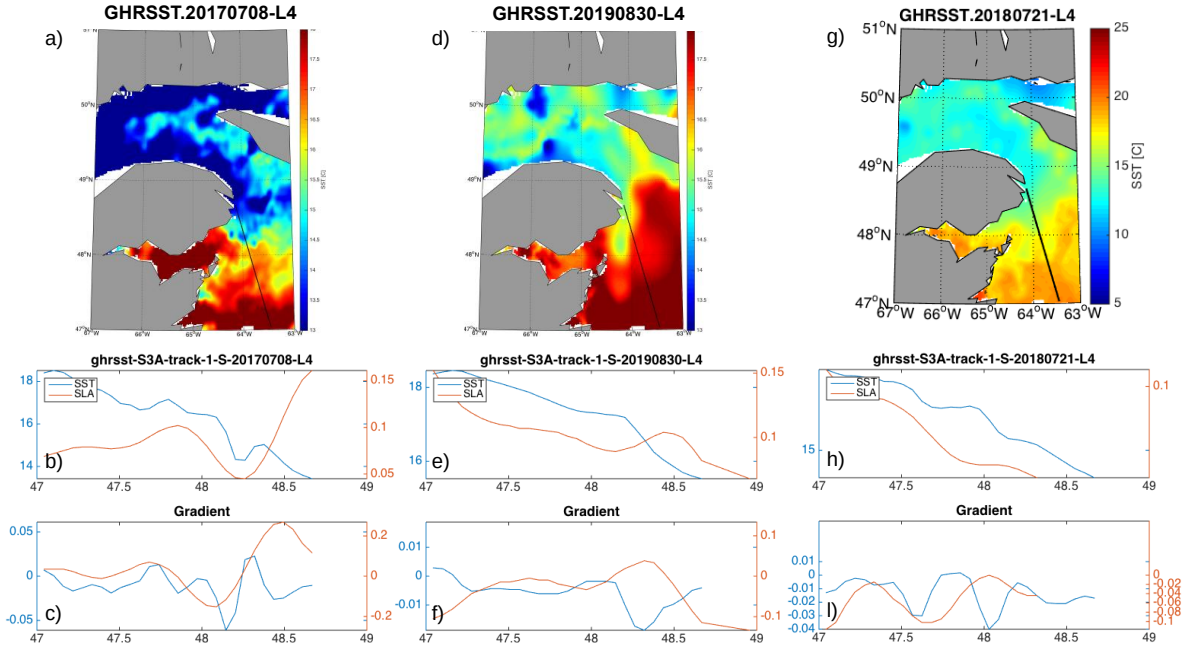

Figure 13. The GHRSST SST distribution on (a) July 8th, 2017, (d) August 30th, 2019 and (g) July 21st, 2018. (b), (e) and (h) latitudinal S3A SLA profile vs. corresponding GHRSST SST along the track (black line in map). (c), (f) and (i) latitudinal SLA gradient vs. SST gradient along the track.

5. Time series

Four indexes were developed to characterize variations of the Gaspé Current in the northwest GSL using 11 years of J2/3 altimetric data. $Index_1$ and $Index_2$ were calculated using the maximum and minimum values of SLA and corresponding locations along each track. Time series of the locations of SLA_{max} and SLA_{min} were grouped based on month (Figure 14). In general, the SLA_{max} was located on the north side, and SLA_{min} was located on the south side. However, reverse profiles were also observed in each month. The averaged location for SLA_{max} gradually moved southward from May to August. Also, the shortest distance between the mean for SLA_{max} and SLA_{min} was found on August (Figure 14d). As mentioned earlier, $Index_1$ [cm/km] is linked to the GC velocity and $Index_2$ [m km] is linked to the water discharge. To examine the inter-annually variation of these indexes, a box plot analysis was used (Figure 15). A box plot provides a simple visualization of summary statistics for the data (Williamson et al., 1989). The bottom and top of each box are the 25th and 75th percentiles of the index in each year, respectively. The distance between the bottom and top of each box is the interquartile range. The red line in the middle of each box is the median. Thus, we can see that the variation in $Index_1$ was higher in 2009-2015 than in 2016-2019 (Figure 15a). Based on 11 years of J2/3 data, the box plot series shows that the monthly variation of $Index_1$ decreases from May to July and then increases to a maximum in September (Figure 15c). For $Index_2$, the variation is high in 2011, 2018 and 2019, and relatively low in 2015 and 2016 (Figure 15b). Overall, it is difficult to say that $Index_2$ has a clear variation (Figure 15d).

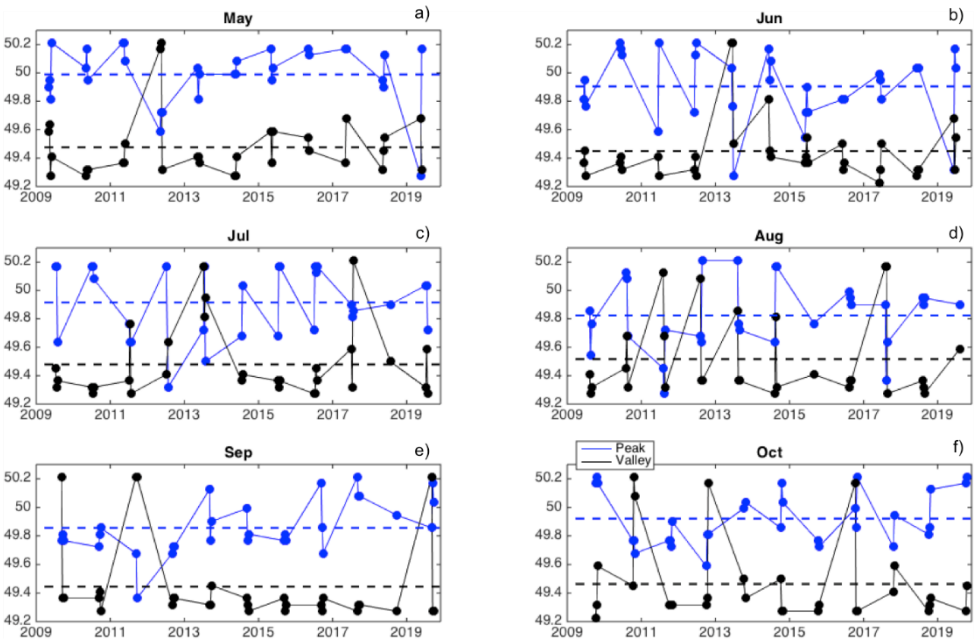

Figure 14. The time series of the location of SLA_{max} (blue dotted line) and SLA_{min} (black dotted line) derived from J2/3 profiles, which have been grouped based on month.

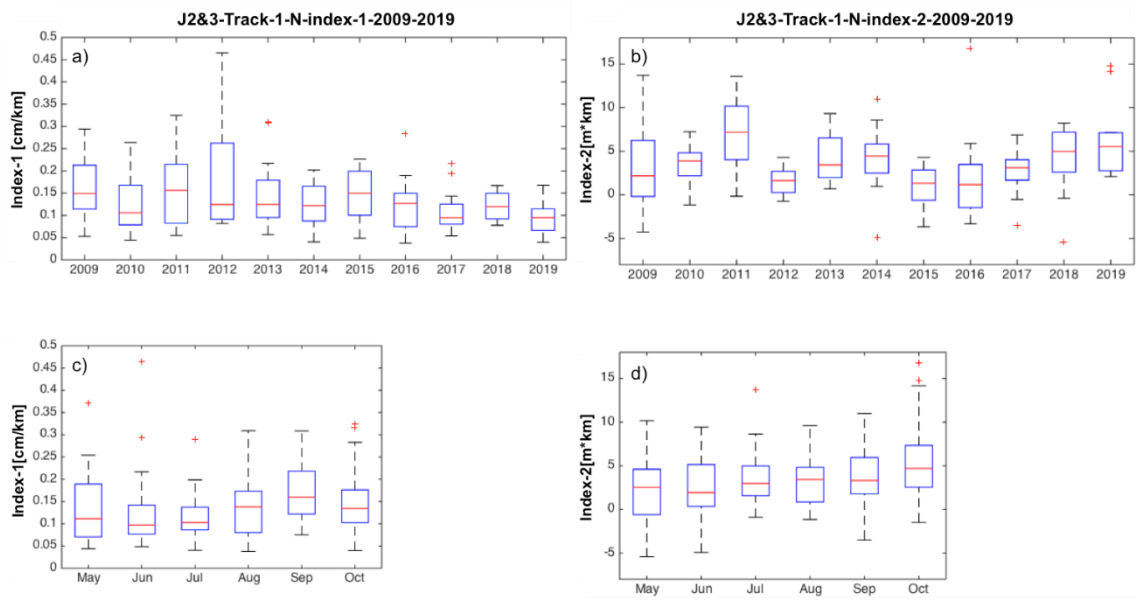

Figure 15. Boxplot diagram series showing the variability of (a) $Index_1$ and (b) $Index_2$ derived from J2/3 SLA profiles from 2009 to 2019. Boxplot series showing the variability of (c) $Index_1$ and (d) $Index_2$ between months, based on 11 years of J2/3 SLA data.

The $Index_{volume}$ was calculated from the J2/3 SLA along the entire north track (Figure 4a), and is linked to the amount of water flowing *through* the track. The time series of $Index_{volume}$ was produced during 2009 to 2019 (Figure 16a). Since the width of the GC can change from 8 km to 17 km (Benoit et al., 1985), $Index_{volume}$ was recalculated by integrating the SLA profile up to N49.5^o (< 25km away from the coastline, Figure 16b). Boxplots showed the inter-annually variation of the $Index_{volume}$ (Figures 17a, 17c). The medium values of $Index_{volume}$ were used to investigate the correlation between $Index_{volume}$ to river discharge (Figures 17b, 17d). The time series of accumulated river discharge from May to October is shown in Figure 18. Since 2002, the monthly runoffs are high in 2011, 2017 and 2019. The runoff in the latter three years is over 80 000 m^3/s. In general, the variation of $Index_{volume}$ is positively correlated with river discharge (R = 0.42, Figure 17b). This result demonstrates that river discharge plays an important role in the ocean dynamics of the northwest GSL. Accounting for the GC width has improved the correlation between the river discharge and $Index_{volume}$ (R = 0.54, Figure 17d). Another index, $index_{slope}$, was calculated using the entire track, which is linked to the GC intensity. The results suggest that the variation of $index_{slope}$ is correlated with river discharge in the spring season (May and June, Figures 19a, 19b).

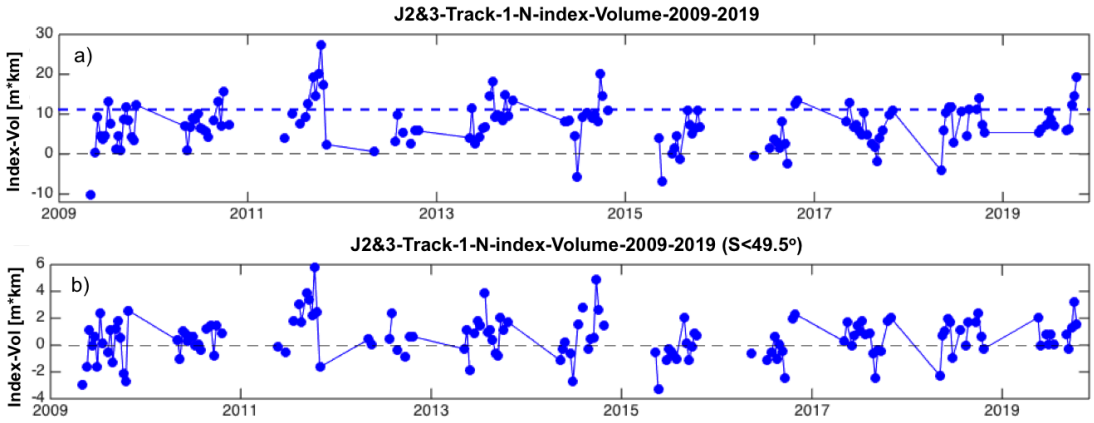

Figure 16. Time series of $Index_{volume}$ derived from entire J2/3 SLA profile during period from 2009 to 2019. (b) Time series of $Index_{volume}$ calculated from the SLA profile up to N49.5º.

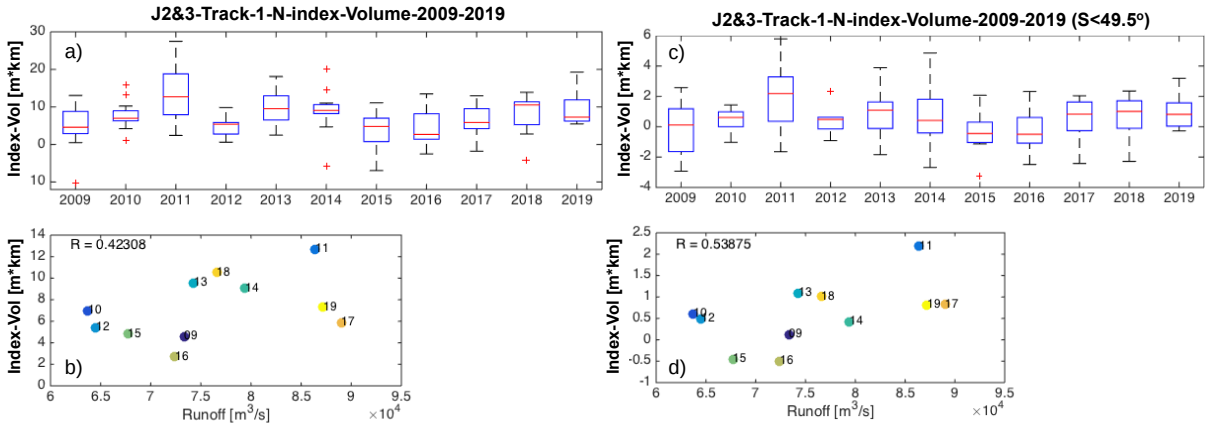

Figure 17. Boxplot series of $Index_{volume}$ derived from (a) entire the J2/3 SLA profile and (c) the SLA profile up to N49.5º during the period from 2009 to 2019. (b) and (d) show scatterplots of the mediums in the boxplots vs. runoff. Points are labeled by year.

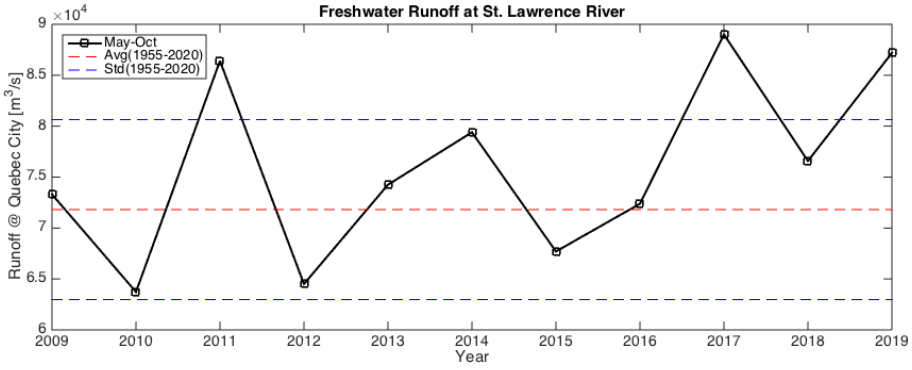

Figure 18. Time series of accumulated St. Lawrence River runoff during May to October over 11 years.

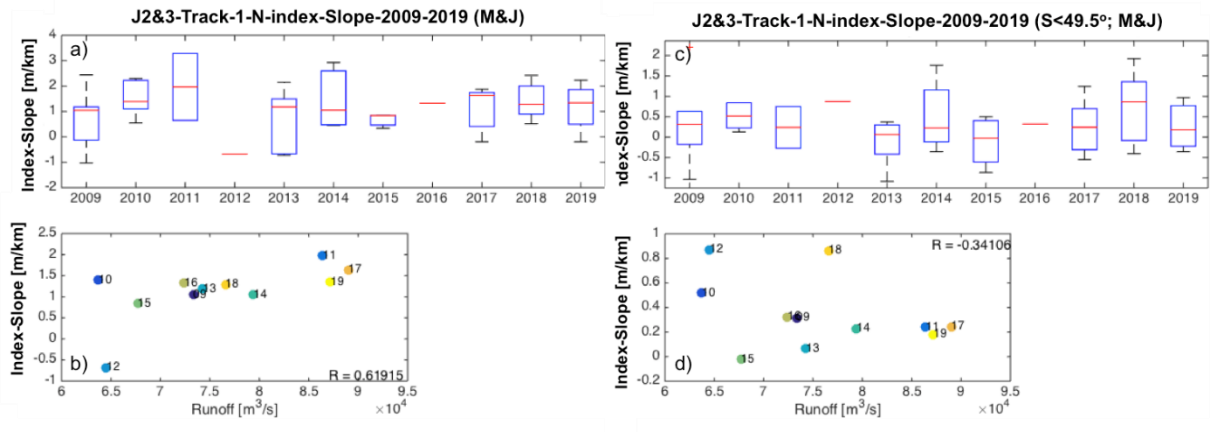

Figure 19. Boxplot series of $Index_{slope}$ derived from (a) entire J2/3 SLA profile and (c) SLA profile up to N49.5º during the period from 2009 to 2019. Only May and June data were used in the boxplot analysis. (b) and (d) show scatterplots of the mediums in the boxplots vs. runoff. Points are labeled by year.

The other two EN tracks on the north branch were also investigated (Figures 4b, 4c, and 9). It is noted that EN track-1N and track-2N are not suitable for an analysis of GC variations since these tracks may not capture the GC. The inter-annual variations of $Index_{volume}$ derived from EN track-1N and EN track-2N are clearly different (Figure 20). One likely reason is that there are only limited EN data available in each year, because the temporal resolution of EN is low (35 days). There is a cyclonic gyre in the northern branch; however, the EN track-1N and track-2N may not fully capture it. Compared with EN tracks, JASON captures the Gaspé Current better as it has more coastal coverage. Therefore, some other appropriate track should be chosen to study oceanic circulation in the northwest GSL.

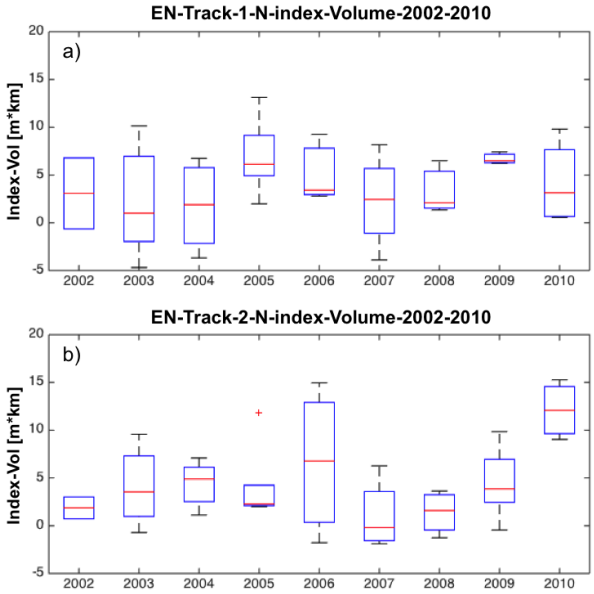

Figure 20. Boxplot series illustrating the variability of $Index_{volume}$ derived from EN along (a) the track-1N and (b) track-2N from 2002 to 2010.

Assuming the location of the SLA_{min} is affected by the GC intensity, the SLA_{min} moves northward when the GC becoming relatively strong. Here, the SLA profiles were removed from analysis when the SLA_{min} was located on the south end of the track, or when SLA_{min} was located further north (> N49.7º). The time series of SLA_{min} derived from J2/3 displays the inter-annual variations during the period from 2009 to 2019 (Fig. 21). The SLA_{min} was located relatively further north in 2011, 2017 and 2019. Also, the medium of the SLA_{min} was located further north in May, when the river discharge reaches its maximum (Figure 21c). It is noted that $Index_2$ and $index_{volume}$ are high in 2011, which occurs when SLA_{min} is further north. This may link to high river discharge in 2011. Furthermore, the monthly sea surface temperature exhibits a high anomaly from May to November over the northwest GSL in 2011 (Galbraith et al., 2012). The buoyancy forcing induced from the freshwater input and heat flux is strong in this year.

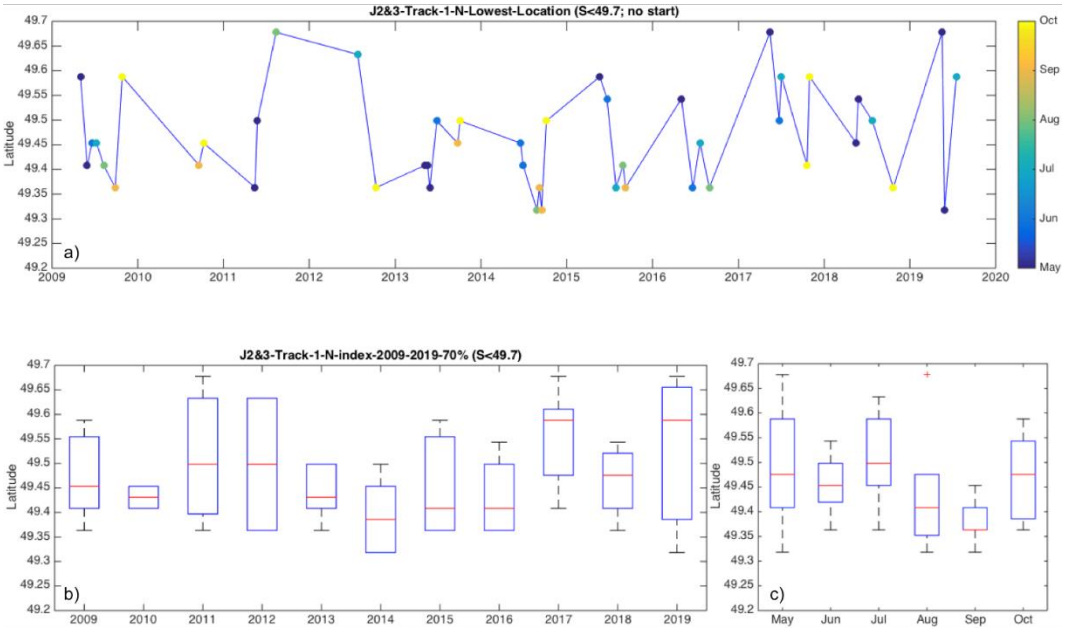

Figure 21. (a) Time series of SLA_{min} location derived from J2/3. (b) Boxplot series displaying the SLA_{min} inter-annual variation during period from 2009 to 2019. (c) Boxplots displaying the monthly SLA_{min} variation.

On the south branch of the northwest GSL, the S3A, S3B and EN altimetry, along – track SLA profiles were combined together to investigate the GC variation (Figure 10). The correlation between the SLA variation and river discharge is weak (Figure 22). Compared with the southern branch, the physical indexes derived from 1-D satellite altimeter data have a better performance in the northern branch. Overall, the results demonstrate that GC variation can be captured by the altimetry data in the northwest GSL. Satellite observations of sea surface height can be utilized to infer the GC variation over long time periods.

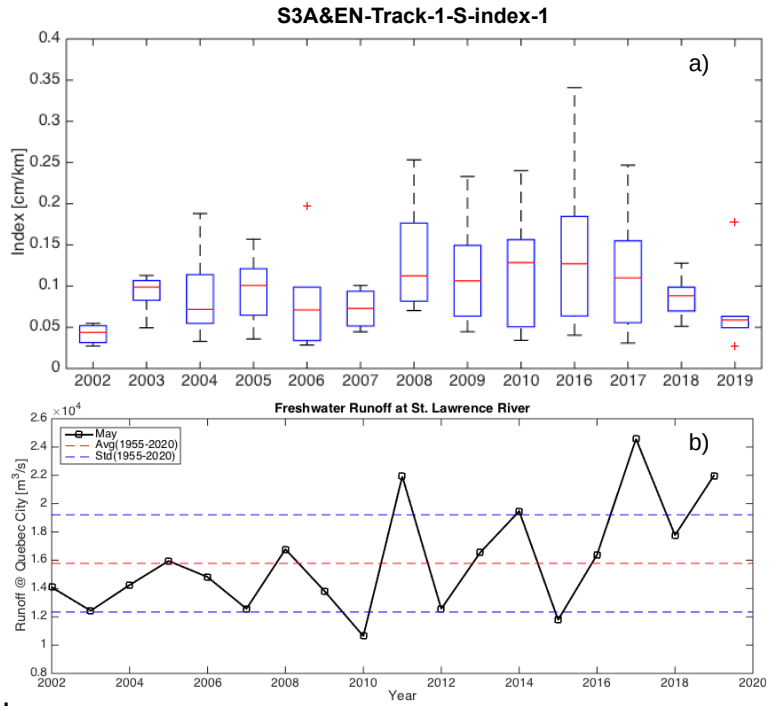

Figure 22. (a) Boxplot series of Index$_1$ derived from S3A and EN SLA profiles during the period from 2002 to 2019. (b) Time series of St. Lawrence River runoff in May from 2002 to 2019.

6. Linking Gaspé Current and zooplankton/whale patterns

6.1 Whale patterns from data

Historical whale sightings are encounters between humans and whales. But the lack of an encounter is only an indication of whale absence, or human absence, or poor observing conditions (e.g., related to fog or rain)*, but not necessarily any one of these alone*. We define a daily index of scatter in the position of whale sightings as the mean distance of individual whales to a mean position within a centered 31-day window,

$$index_{scatter} = \sum_{-15\ days}^{+15\ days} \frac{position - mean\ position}{number\ of\ individual\ whales}, \qquad (8)$$

where mean position is the average latitude and longitude of all sightings in the database. Figure 23 reveals a dramatic increase in the number of sightings before and after 2017. If variations in human presence (or sighting efforts) and sighting conditions can be ignored, then small counts and large scatter suggest that there are fewer whales traveling less frequently in groups; whereas large counts and small scatter suggest more whales traveling more frequently in groups. These distinctions might even be extended to differences in whale age and sex (e.g., with younger whales in the latter, larger whale groups). The number of sightings generally peaks in July, although sightings in 2017 and 2019 have extended well into November.

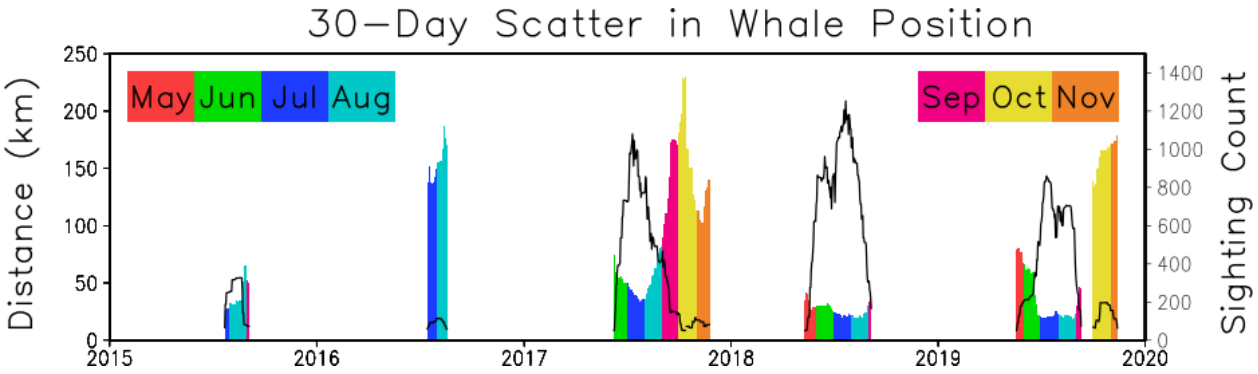

Figure 23. Histogram of the average distance between all blue and right whale sightings and a fixed sightings position (i.e., the average position over all months; black square in Figure 24), as given by a daily scatter index with sightings from a centered 31-day moving window. Distance is coloured by month between 2015 and 2020 and the number of individual whales sighted (black line) is included.

Figure 24 illustrates the mean position (black dot) and scatter index (lower left value in each panel) for summer months between 2016 and 2019, as given by the combined NARWC (Kenny 2019) and DFO (2020) database. There has been a tendency for sightings to begin somewhat earlier each year from 2015 (not shown) to 2018. But in 2019 sightings occurred later; however, to date, 2019 and 2020 sightings continue to be assembled. Fewer sightings are apparent in 2015 and 2016, with a large increase in encounters starting in the summer of 2017. The scatter index is consistent with more disperse sightings occurring during the summer of 2016, towards the end of the 2017 of summer, and at the beginning of the 2018 and 2019 summers. Monthly estimates of Chlorophyll-a concentration, based on a number of ocean colour satellite estimates (CMEMS_009_082), are included in Figure 24. However, apart from concentrations being high during the summer months of 2017, both near to and away from the coast, there seems to be little to indicate changes in sightings at large spatiotemporal scales that link to Chlorophyll-a concentrations.

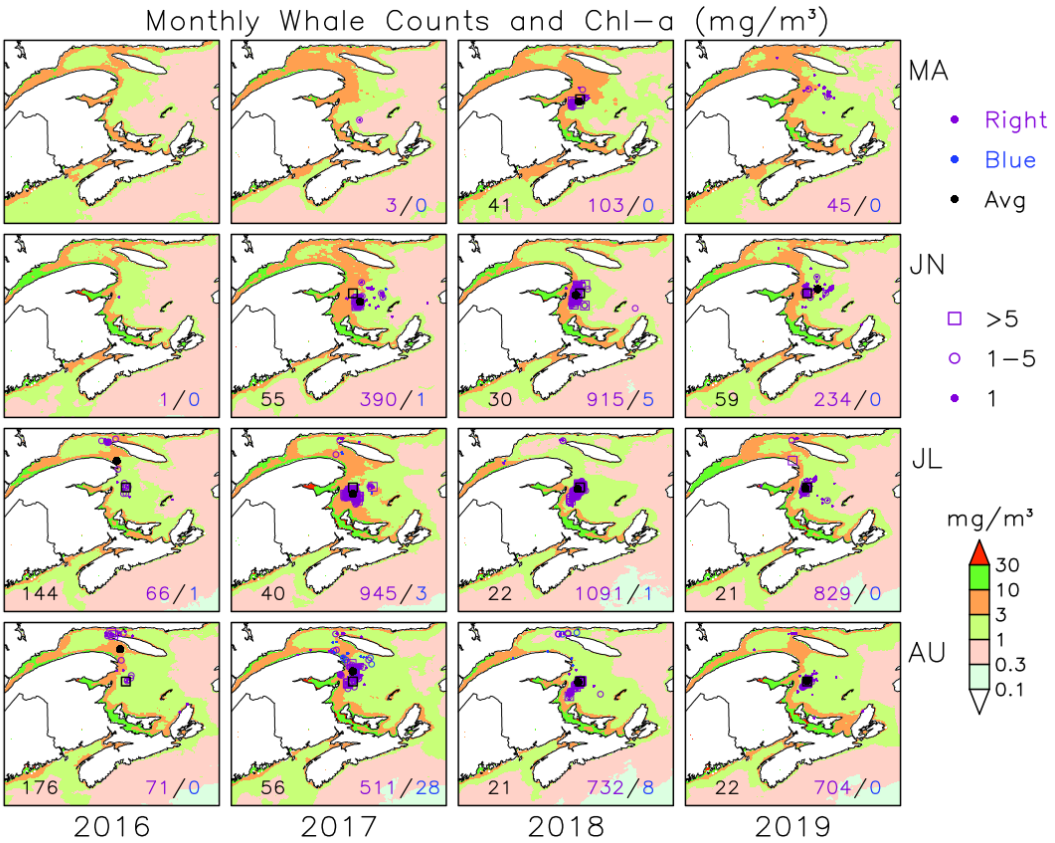

Figure 24. Monthly counts of the estimated number of right and blue whales sighted during May-August (ordinate) during 2016-2019 (abscissa). Numerical values in each panel are the mean distance of individual whales (black, in 10^3 km) to a fixed average position for all months (the black square; a black dot shows the average position for individual months), and number of right (purple) and blue (blue) whales. Included are monthly estimates of Chlorophyll-a concentration (mg/m^3) based on a number of ocean colour satellite estimates (CMEMS_009_082). Note that multiple observers may count an individual whale more than once, either on the same day or on different days.

6.2 Zooplankton temporal patterns from literature

DFO's recent CSAS (Canadian Science Advisory Secretariat) report (Blais et al. 2021) provides a detailed summary of *Calanus finmarchicus,* zooplankton, and biomass variations along different routinely sampled transects and stations in the Gulf of St. Lawrence. Figure 25 shows temporal variations of five different zooplankton indices from high frequency zooplankton sampling at Shediac Valley station (47.78°N, 64.03°W). This station is chosen for analysis as it is in the area of the whale habitat. This station was sampled primarily in late spring (e.g. May), summer and fall. As zooplankton samples are collected over the entire water column, zooplankton indices represent depth-integrated metrics. The zooplankton concentration shows different variation characteristics. From 2014-2017, zooplankton concentrations show consistent decreasing trends, except *Calanus finmarchicus*. *Calanus finmarchicus* is a major component of the NARW prey (Brennan et a., 2021; Sorochan et al., 2021), which basically been flat from

2014 through 2019, with exception of a strong decline in 2015 and a slight decline in 2017. There was a bounce back of three zooplankton variables (biomass, *pseudocalanus* and total-copepods) in 2018, then drop down again in 2019. The biomass and zooplankton concentrations in 2017 were mostly below normal (anomaly value <0).

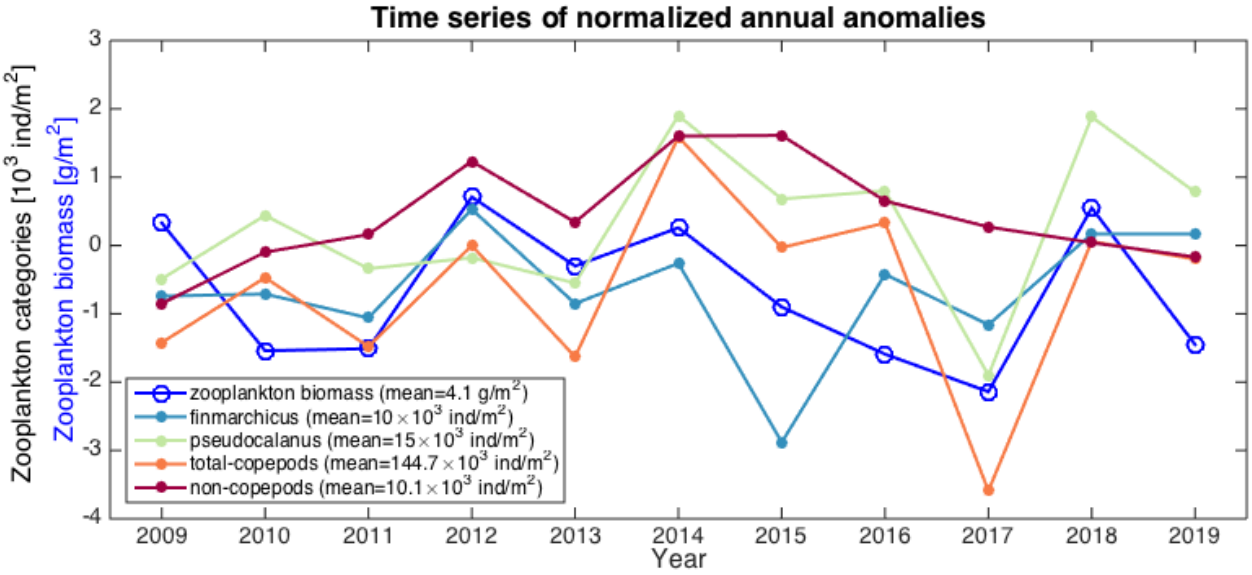

Figure 25. Temporal variations of different zooplankton indices anomalies at Shediac Valley station. The five indices include: total zooplankton biomass, *Calanus finmarchicus*, *Pseudocalanus*, total-copepods, and non-copepods. Anomalies are given relative to means for the 1999-2015 reference period that are shown in the legend. Note that all copepod indices exhibit low anomalies in 2017 and 2019 [data digitized from Blais et al., 2021].

6.3 River discharge pattern at Neuville, QC

River runoff estimates at Neuville QC include fresh water input from all rivers upstream. Although this is a small component of the water flow in the St. Lawrence Estuary, it exerts a fundamental control on stratification and dynamical forcing for the Gaspé Current (Koutitonsky and Bugden 1991). Numerical simulations confirm the dominant role of river runoff on the flow pattern of the Gaspé Current (e.g., Sheng 2001). A seasonal increase in St. Lawrence river discharge typically results in a stronger Gaspé Current (up to ~ 0.1m/s) (Ohashi and Sheng, 2013). Figure 26a shows the river discharge timeseries for 1955-2020. In particular, the latest available five years are presented as an individual and average monthly timeseries in Figures 26b,26c. The dominant characteristic is seasonal variability, where June is the month with the highest river run-off of the year. Most years also feature a second but much lower peak river runoff in the late fall, around November. The river runoff also shows strong inter-annual variability. During 2015-2020, the years 2017 and 2019 had much higher runoff than the other three years.

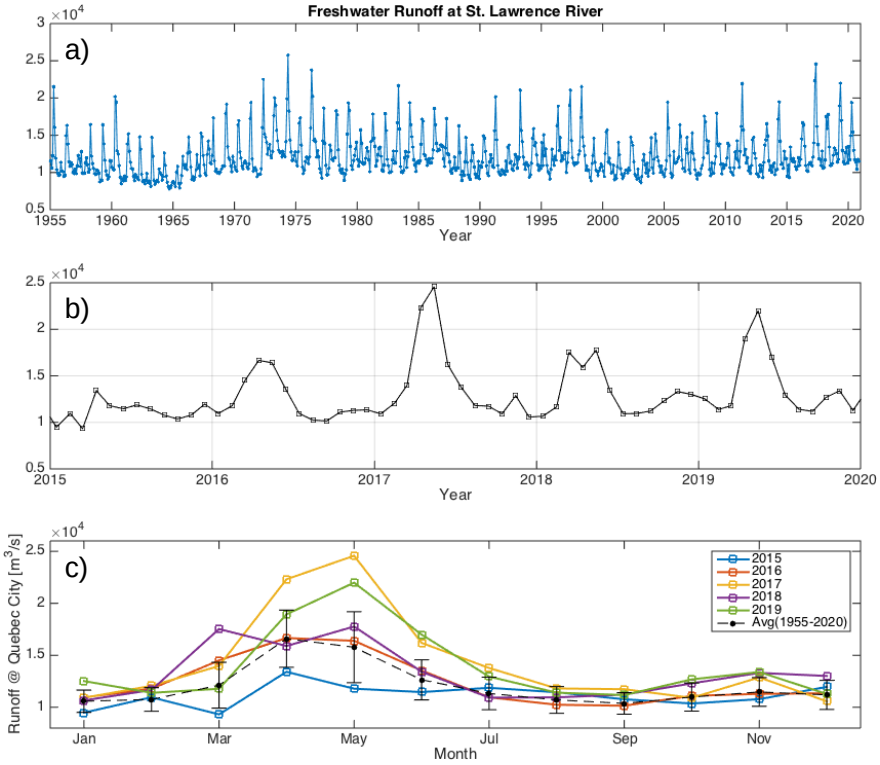

Figure 26. Time series of St. Lawrence River runoff during (a) 1955 to 2020, (b) 2015 to 2019, and (c) seasonal variation in monthly average runoff for the years 2015 to 2019. Black dotted curve shows the monthly mean and standard deviation based on 65 years (1955-2020) of runoff data.

6.4 Correlation analysis

In summary, we have compiled time series data for river run-off, whale scatter index, zooplankton concentration, and the physical indexes developed in this project (Figure 27). Pearson correlation analysis among indexes using annual data (2009 to 2019) are shown in the Appendix.

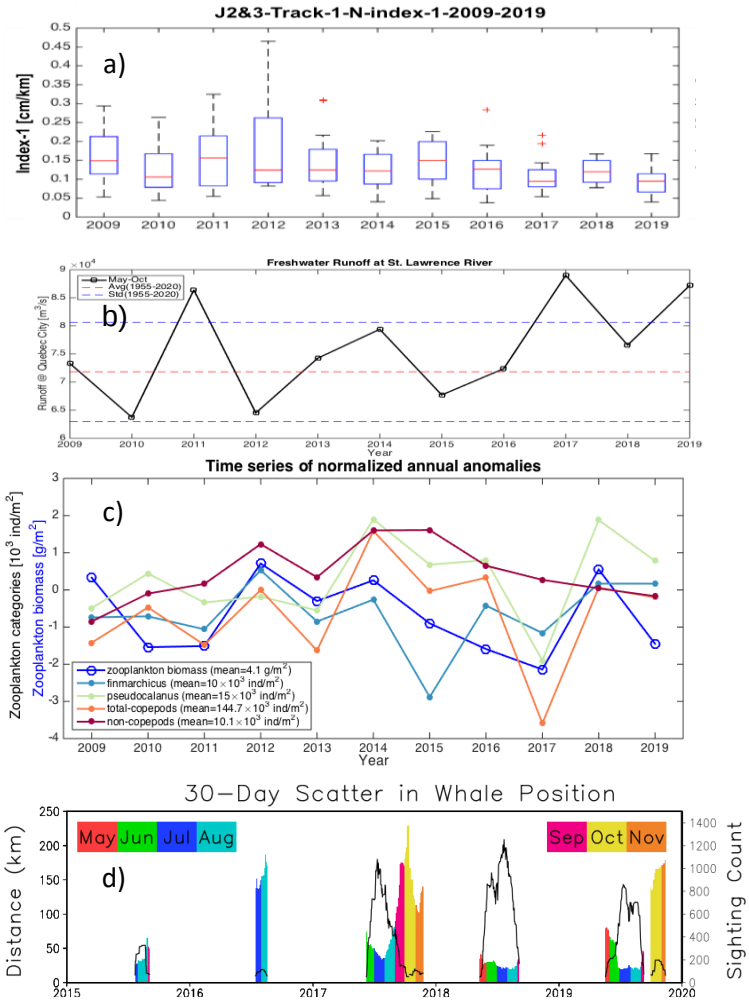

Figure 27. Compiled plots of different parameters: (a) physical $Index_1$ (b) river discharge, (c) zooplankton concentration (d) whale sightings scatter index.

The physical $Index_1$ appears to shows a negative correlation with river run-off data (Figures 27 and A1, R=-0.46). As $Index_1$ is a proxy for the Gaspé Current intensity, it is suggested that $Index_1$ captures the driving force of the Gaspé Current due to upstream river run-off. $Index_1$ also shows positive correlation with zooplankton biomass (Figure 27 and A1, R=0.55). Zooplankton peaks in 2010, 2016 exist at both western and southern locations; but are not fully captured by $Index_1$. This seems to suggest biological blooming in these years, rather than purely physical drivers. $Index_1$ shows good correlation with the scatter index in 2017 to 2019 (Figures 27a and 27d). Low values for $Index_1$ appear to correlate to scattered whale sightings, for example, in years 2017 and 2019.

Overall, all the parameters appear to correlate to each other reasonably well (Figure 27 and Appendix 1). $Index_1$ is able to capture the main pattern of variations of the physical conditions in the whale habitat ecosystem (zooplankton biomass, *Calanus finmarchicus* abundance and river

discharge), and therefore can potentially be used as an indicator of zooplankton conditions and whale scatter patterns. The correlation among other physical and zooplankton variables should be investigated in the future work.

7. Summary and future perspectives

Physical indexes are developed from remote sensing data to monitor variations of the Gaspé Current, a dominant ocean circulation process in the western Gulf of St. Lawrence (GSL) circulation. The variations of physical indexes are found to correlate reasonably well with the river run-off of the St. Lawrence Estuary, the distribution patterns of both zooplankton and also North Atlantic Right Whales in the GSL. These indexes are helpful to understand historical variations in the physical conditions in the whale habitat, and therefore can be useful to predict whale gathering patterns in the near future, providing a new tool for the management of whale habitat in the GSL.

Future focus of this work will be to automate the process and methodology for developing physical indexes from altimeter and synthetic aperture radar (SAR), to allow operational applications. This will lead to a capability to study the predictability and performance of these physical indexes to predict whale habitat suitability for the coming seasons.

The physical indexes developed in this report provide a unique synergy of information, combining complex remote sensing measurements of the intricate whale habitat ecosystem. The index includes observations from sea level height and sea surface roughness, which in turn, are subject to complex modulations due to multiple factors, such as the complicated ocean circulation system in the Gulf of St. Lawrence, wind stress and wave – induced upper ocean mixing, air-sea interactions, land-sea interactions, oceanic mesoscale / submesoscale dynamics etc. The physical indexes provide another layer of data and a tool for the understanding and managing the fisheries in the complex whale habitat ecosystem.

Acknowledgements

We thank Catherine Johnson, Stéphane Plourde, Joël Chassé, Jean-François, Gosselin, Valérie Harvey, Sheila Prall-Dillman, Lindsay Weber, Hilary Moors-Murphy, Angelia Vanderlaan from DFO sciences and colleagues of the Marine mammal management team in the National Headquarter, for their expert advice and insightful discussions. We thank data agencies for providing data available to this project: whale sightings database from North Atlantic Right Whale Consortium and from DFO sciences Maritimes region; synthetic aperture radar (SAR) from Canadian Space Agency; Altimeter data from Copernicus CMEMS data center; river discharge data from the St. Lawrence Global Observatory. This study is funded by DFO's Competitive Science Research Fund (CSRF), and Species at Risk (SAR).

Appendix

A Correlation Matrix between discharge, index$_1$ and zooplankton indices.

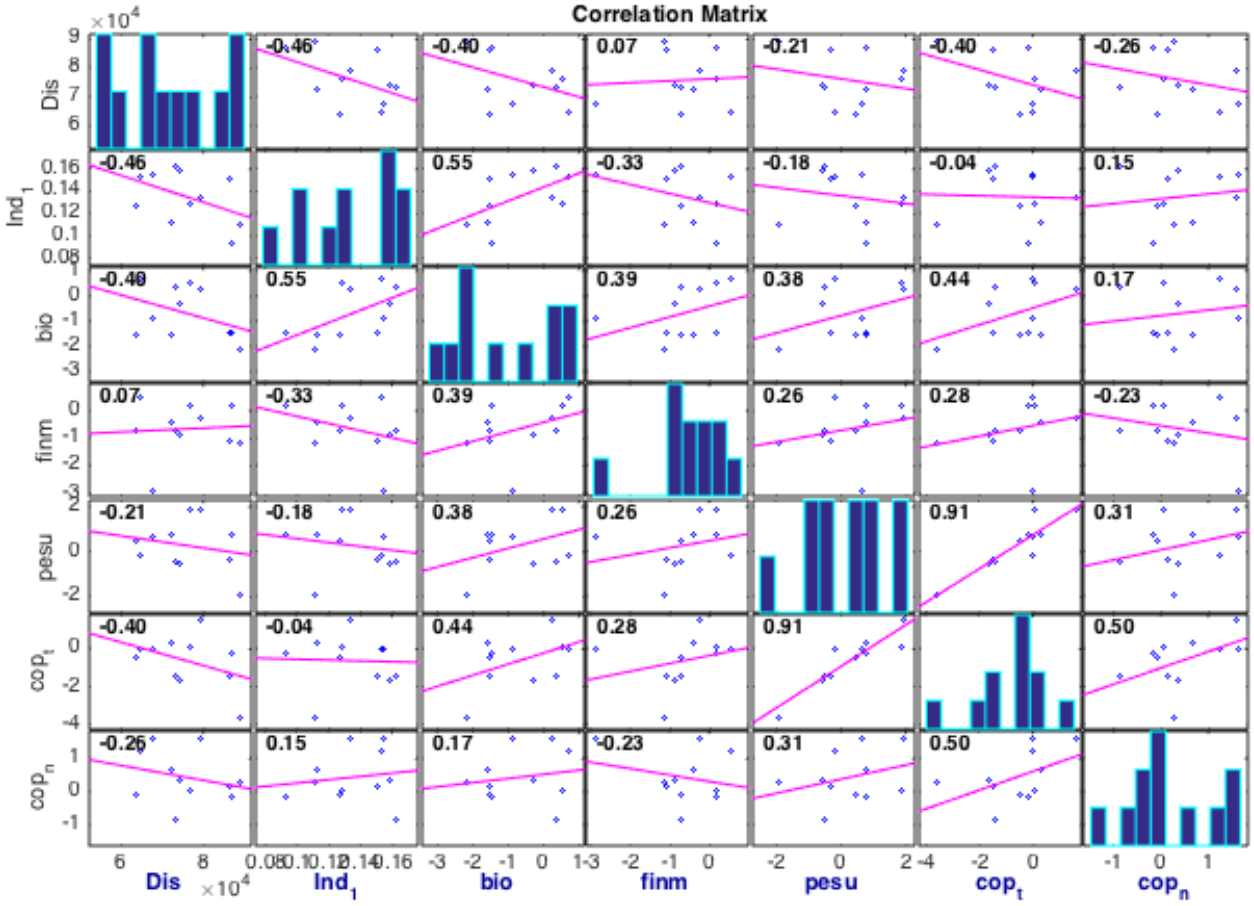

Figure A1. Correlation scatterplots for discharge, index$_1$ and zooplankton indexes using data from 2009 to 2019. Here, we use the following abbreviations:

Dis	river discharge
Ind$_1$	Index$_1$
bio	total zooplankton biomass
finm	*calanus finmarchicus*
pseu	*pseudocalanus* spp.
cop$_t$	total-copepods
cop$_n$	non-copepods
R	correlation coefficient

References

Benoit, J., El-Sabh, M. I., and Tang, C. L. 1985. Structure and seasonal characteristics of the Gaspé Current. Journal of Geophysical Research: Oceans, 90(C2), 3225-3236.

Bourgault, D., & Koutitonsky, V. G. 1999. Real-time monitoring of the freshwater discharge at the head of the St. Lawrence Estuary. Atmosphere-Ocean, 37(2), 203-220.

Bonjean, F., & Lagerloef, G. S. 2002. Diagnostic model and analysis of the surface currents in the tropical Pacific Ocean. Journal of Physical Oceanography, 32(10), 2938-2954.

Brennan C. E., Maps F., Gentleman W. C., et al. 2019. How transport shapes copepod distributions in relation to whale feeding habitat: Demonstration of a new modelling framework. Progress in Oceanography,171:1-21.

Brennan, C. E., Maps, F., Gentleman, W. C., Lavoie, D., Chassé, J., Plourde, S., and Johnson, C. L. 2021. Ocean circulation changes drive shifts in Calanus abundance in North Atlantic right whale foraging habitat: a model comparison of cool and warm year scenarios. Progress in Oceanography, 197, 102629.

Blais, M., Galbraith, P.S., Plourde, S., Devine, L. and Lehoux, C. 2021. Chemical and Biological Oceanographic Conditions in the Estuary and Gulf of St. Lawrence during 2019. DFO Can. Sci. Advis. Sec. Res. Doc. 2021/002. iv + 66 p.

CMEMS, 2020. Sea Level Thematic Assembly Centre (SL-TAC) quality information document, available at http://marine.copernicus.eu/documents/QUID/CMEMS-SL-QUID-008-032-062.pdf (accessed 2 January 2021).

Cox, C., and Munk, W. 1954. Measurement of the roughness of the sea surface from photographs of the Sun's glitter, J. Opt. Soc. Am., 44, 838–850, doi:10.1364/JOSA.44.000838.

Cox, S. L., Embling C. B., Hosegood P.J., Votier, S.C., Ingram, S. N. 2018. Oceanographic drivers of marine mammal and seabird habitat-use across shelf-seas: A guide to key features and recommendations for future research and conservation management. Estuarine, Coastal and Shelf Science, 212:294-310.

Cullen, J.J., Franks, P.J.S., Karl, D.M., Longhurst, A. 2002. Physical influences on marine ecosystem dynamics. The Sea.12:297-336.

Dal-SONOBUOY. (n.d.). https://www.dal.ca/news/2018/09/25/armed-with-data--unprecedented-experiment-with-canadian-military.html

Davies, K.T.A., Taggart C.T., Smedbol, R.K. 2014. Water mass structure defines the diapausing copepod distribution in a right whale habitat on the Scotian Shelf. Marine Ecology Progress Series. 497:69-85.

de Lafontaine, Y., Demers, S., and Runge, J. 1991. Pelagic food web interactions and productivity in the Gulf of St Lawrence: a perspective, pp. 99-123. In The Gulf of St Lawrence: Small Ocean or Big Estuary? Ed. by J-C. Therriault. Canadian Special Publication of Fisheries and Aquatic Sciences, 113.

DFO, 2020: Whale-Sightings Database, Team Whale, Bedford Institute of Oceanography (accessed 2 December 2020).

El-Sabh, M. I. 1976. Surface circulation pattern in the Gulf of St. Lawrence. Journal of the Fisheries Board of Canada, 33(1), 124-138.

Fu, L. L., and Chelton, D. B. 2001. Large-scale ocean circulation. In International Geophysics (Vol. 69, pp. 133-viii). Academic Press.

Gavrilchuk, K., Lesage, V., Fortune, S., Trites, A.W., Plourde, S. 2020. A mechanistic approach

to predicting suitable foraging habitat for reproductively mature North Atlantic right whales in the Gulf of St. Lawrence. Vol 34: Canadian Science Advisory Secretariat.

Han, G. 2004. Sea level and surface current variability in the Gulf of St Lawrence from satellite altimetry. International Journal of Remote Sensing, 25(22), 5069-5088.

Joseph, A. 2013. Measuring ocean currents: tools, technologies, and data. Newnes.

Johnson, C.L., Leising, A.W., Runge, J.A., et al. 2007. Characteristics of Calanus finmarchicus dormancy patterns in the Northwest Atlantic. ICES Journal of Marine Science. 65(3):339-350.

Kenney, R.D. 2019. The North Atlantic Right Whale Consortium database: A guide for users and contributors, available at https://www.narwc.org/uploads/1/1/6/6/116623219/narwc_users_guide__v6.pdf.

Kudryavtsev, V., Myasoedov, A., Chapron, B., Johannessen, J. A., and Collard, F. 2012. Imaging mesoscale upper ocean dynamics using synthetic aperture radar and optical data, J. Geophys. Res., 117, C04029, doi:10.1029/2011JC007492.

Koch, W. 2004. Directional analysis of SAR images aiming at wind direction, IEEE Trans. Geosci. Remote Sens., 42, doi:10.1109/TGRS.2003.818811.

Koutitonsky, V. G. and Bugden, G. L. 1991. The physical oceanography of the Gulf of St. Lawrence: a review with emphasis on the synoptic variability of the motion, p.57-90. The Gulf of St. Lawrence: small ocean or big estuary? Can. Spec. Publ. Fish. Aquat. Sci. 113.

Lehoux, C., Plourde, S., Lesage, V. 2020. Significance of dominant zooplankton species to the North Atlantic Right Whale potential foraging habitats in the Gulf of St. Lawrence. Vol 033: Canadian Science Advisory Secretariat.

Maps, F., Plourde, S., Lavoie, D., McQuinn, I.H., Chasse, J.D. 2014. Modelling the influence of daytime distribution on the transport of two sympatric krill species (Thysanoessa raschii and Meganyctiphanes norvegica) in the Gulf of St Lawrence, eastern Canada. Ices Journal of Marine Science.71:282-292.

McQuinn, I.H., Plourde, S., Pierre, J.-F.S., Dion, M. 2015. Spatial and temporal variations in the abundance, distribution, and aggregation of krill (Thysanoessa raschii and Meganyctiphanes norvegica) in the lower estuary and Gulf of St. Lawrence. Progress in Oceanography. 131:159-176.

Meyer-Gutbrod, E.L., Greene, C.H. 2018. Uncertain recovery of the North Atlantic right whale in a changing ocean. Global change biology. 24(1):455-464.

NOAA, 2004. Synthetic Aperture Radar Marine User's Manual, C. R. Jackson and J. R. Apel, Eds., available at https://www.sarusersmanual.com.

Prairie, J.C., Sutherland, K.R., Nickols, K.J., Kaltenberg, A.M. 2012. Biophysical interactions in the plankton: A cross-scale review. Limnology and Oceanography: Fluids and Environments. 2(1):121-145.

Plourde, S., Runge, J.A. 1993. Reproduction of the planktonic copepod Calanus finmarchicus in the Lower St. Lawrence Estuary: relation to the cycle of phytoplankton production and evidence for a Calanus pump. Mar. Ecol. Prog. Ser. 102(3):217-227.

Plourde, S., Lehoux, C., McQuinn, I.H., Lesage, V. 2016. Describing krill distribution in the western North Atlantic using statistical habitat models. Vol 111: Canadian Science Advisory Secretariat.

Plourde, S., Joly, P., Runge, J.A., Zakardjian, B., Dodson, J.J. 2001. Life cycle of Calanus finmarchicus in the lower St. Lawrence Estuary: the imprint of circulation and late timing of the spring phytoplankton bloom. Canadian Journal of Fisheries and Aquatic Sciences. 58(4):647-658.

Plourde, S., Lehoux, C., Johnson, C.L., Perrin, G., Lesage, V. 2019. North Atlantic right whale (Eubalaena glacialis) and its food: (I) a spatial climatology of Calanus biomass and potential

foraging habitats in Canadian waters. Journal of Plankton Research. 41(5):667-685.

Radford, S.F., Gran, R.L., Miller, R.V. 1994. Detection of whale wakes with synthetic aperture radar. Marine Technology Society journal. 28(2):46-52.

Rio, M.-H., Mulet, S., Picot, N., 2014. Beyond GOCE for the ocean circulation estimate: synergetic use of altimetry, gravimetry, and in situ data provides new insight into geostrophic and Ekman currents. Geophys. Res. Lett. 41. https://doi.org/10.1002/2014GL061773.

Roy, S., Silverberg, N., Romero, N., Deibel, D., Klein, B., Savenkoff, C., Vezina, A. F., et al. 2000. Importance of mesozooplankton feeding for the downward flux of biogenic carbon in the Gulf of St Lawrence (Canada). Deep-Sea Research II, 47: 519-544.

SARA listed species recovery measures. In: Fisheries and Oceans, Canada. 2020.

Shen, H., Perrie, W., Johnson, C.L. 2020. Predicting internal solitary waves in the Gulf of Maine. Journal of Geophysical Research: Oceans.125(3):e2019JC015941.

Sheng, J. 2001. Dynamics of a buoyancy-driven coastal jet: The Gaspé Current. Journal of Physical Oceanography, 31(11), 3146-3162.

SmartWhale initiative. https://buyandsell.gc.ca/procurement-data/tender-notice/PW-MTB-450-15781. Accessed Jul.10, 2020

Sorochan, K.A., Plourde, S., Baumgartner, M.F. and Johnson, C.L. 2021. Availability, supply, and aggregation of prey (Calanus spp.) in foraging areas of the North Atlantic right whale (Eubalaena glacialis). ICES Journal of Marine Science.

The Marine Ecological Time Series database. https://www.st.nmfs.noaa.gov/copepod/time-series/ca-50702/

Wang, Z., Shen, H., Heaslip, S., Gerfrey, N. 2020. Physical Oceanography in the Fundian Channel-Browns Bank Area of Interest (AOI). In: Biophysical and Ecological Overview of the Fundian Channel-Browns Bank Area of Interest (AOI). Canadian Science Advisory Secretariat.

Waite, A. M., Raes, E., Beckley, L. E., Thompson, P. A., Griffin, D., Saunders, M., Säwström, C., O'Rorke, R., Wang, M., Landrum, J. P., and Jeffs, A. 2019. Production and ecosystem structure in cold-core vs. warm-core eddies: Implications for the zooplankton isoscape and rock lobster larvae, Limnol. Oceanogr., 64, 2405-2423, doi:10.1002/lno.11192.

Williamson, D. F., Parker, R. A., and Kendrick, J. S. 1989. The box plot: a simple visual method to interpret data. Annals of internal medicine, 110(11), 916-921.

WhaleMap. http://whalemap.ocean.dal.ca. Accessed Jul.10, 2020.

Yu, Y., Wang, L., and Li, Z. 2014. Geostrophic current estimation using altimetric cross-track method in northwest Pacific. In IOP Conference Series: Earth and Environmental Science (Vol. 17, No. 1, p. 012105). IOP Publishing.

Zooplankton Database. https://www.dfo-mpo.gc.ca/science/data-donnees/plankton-plancton/basedonnees-zooplankton-database-eng.html. Accessed Jul.10, 2020.